

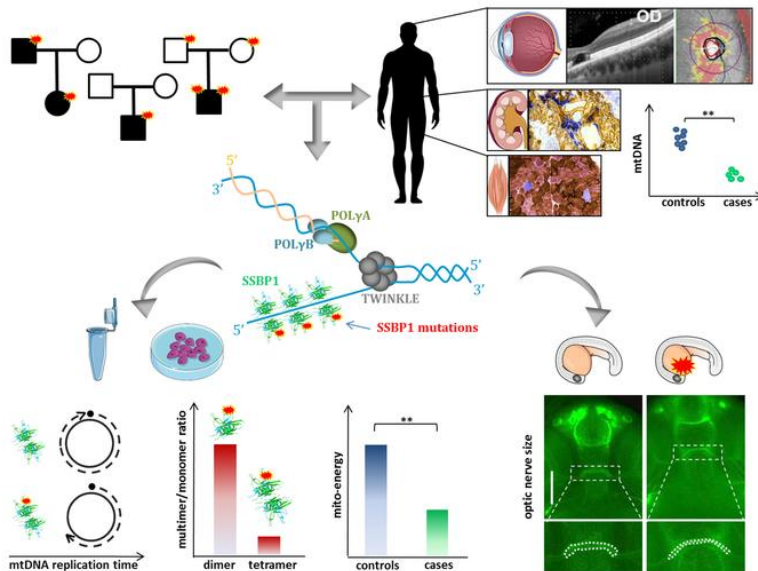
## SSBP1 mutations cause mtDNA depletion underlying a complex optic atrophy disorder

Valentina Del Dotto, ... , Tommaso Pippucci, Valerio Carelli

*J Clin Invest.* 2019. <https://doi.org/10.1172/JCI128514>.

Research In-Press Preview Genetics Ophthalmology

### Graphical abstract



Find the latest version:

<https://jci.me/128514/pdf>



## **SSBP1 mutations cause mtDNA depletion underlying a complex optic atrophy disorder**

Valentina Del Dotto,<sup>1\*</sup> Farid Ullah,<sup>2,3,4\*</sup> Ivano Di Meo,<sup>5\*</sup> Pamela Magini,<sup>6\*</sup> Mirjana Gusic,<sup>7,8</sup> Alessandra Maresca,<sup>9</sup> Leonardo Caporali,<sup>9</sup> Flavia Palombo,<sup>9</sup> Francesca Tagliavini,<sup>9</sup> Evan Harris Baugh,<sup>10</sup> Bertil Macao,<sup>11</sup> Zsolt Szilagyi,<sup>11</sup> Camille Peron,<sup>5</sup> Margaret A. Gustafson,<sup>12</sup> Kamal Khan,<sup>2,3,4</sup> Chiara La Morgia,<sup>1,9</sup> Piero Barboni,<sup>13</sup> Michele Carbonelli,<sup>9</sup> Maria Lucia Valentino,<sup>1,9</sup> Rocco Liguori,<sup>1,9</sup> Vandana Shashi,<sup>14</sup> Jennifer Sullivan,<sup>14</sup> Shashi Nagaraj<sup>15</sup>, Mays El-Dairi,<sup>16</sup> Alessandro Iannaccone,<sup>17</sup> Ioana Cutcutache,<sup>18</sup> Enrico Bertini,<sup>19</sup> Rosalba Carrozzo,<sup>19</sup> Francesco Emma,<sup>20</sup> Francesca Diomedi-Camassei,<sup>21</sup> Claudia Zanna,<sup>22</sup> Martin Armstrong,<sup>23</sup> Matthew Page,<sup>18</sup> Nicholas Stong,<sup>10</sup> Sylvia Boesch,<sup>24</sup> Robert Kopajtich,<sup>7,8</sup> Saskia Wortmann,<sup>7,8,25</sup> Wolfgang Sperl,<sup>25</sup> Erica E. Davis,<sup>2</sup> William C. Copeland,<sup>12</sup> Marco Seri,<sup>6,26</sup> Maria Falkenberg,<sup>11</sup> Holger Prokisch,<sup>7,8#</sup> Nicholas Katsanis,<sup>2,27,28#</sup> Valeria Tiranti,<sup>5#</sup> Tommaso Pippucci,<sup>6#&</sup> Valerio Carelli<sup>1,9#&</sup>

<sup>1</sup>Unit of Neurology, Department of Biomedical and NeuroMotor Sciences (DIBINEM), University of Bologna, Italy.

<sup>2</sup>Center for Human Disease Modeling, Duke University, Durham, NC 27701, USA.

<sup>3</sup>Human Molecular Genetics Laboratory, Health Biotechnology Division, National Institute for Biotechnology and Genetic Engineering (NIBGE), Pakistan.

<sup>4</sup>Pakistan Institute of Engineering and Applied Sciences (PIEAS), Faisalabad, Pakistan.

<sup>5</sup>Unit of Medical Genetics and Neurogenetics, Fondazione IRCCS Istituto Neurologico C. Besta, Milan, Italy.

<sup>6</sup>Medical Genetics Unit, Sant'Orsola-Malpighi University Hospital, Bologna, Italy.

<sup>7</sup>Institute of Human Genetics, Helmholtz Zentrum München, Neuherberg, Germany.

<sup>8</sup>Institute of Human Genetics, Technische Universität München, Munich, Germany.

<sup>9</sup>IRCCS Istituto delle Scienze Neurologiche di Bologna, UOC Clinica Neurologica, Bologna, Italy.

<sup>10</sup>Institute for Genomic Medicine, Columbia University, New York, NY.

<sup>11</sup>Department of Medical Biochemistry and Cell Biology, Institute of Biomedicine, University of Gothenburg, Gothenburg SE-405 30, Sweden.

<sup>12</sup>Genome Integrity and Structural Biology Laboratory, National Institute of Environmental Health Sciences, Research Triangle Park, NC 27709 USA.

<sup>13</sup>Department of Ophthalmology, Studio Oculistico d'Azeglio, Bologna, Italy.

<sup>14</sup>Division of Medical Genetics, Department of Pediatrics, Duke University School of Medicine, Durham, NC, USA.

<sup>15</sup>Division of Nephrology, Department of Pediatrics, Duke University School of Medicine, Durham, NC, USA.

<sup>16</sup>Duke Eye Center, Neuro-Ophthalmology Service, Duke University School of Medicine, Durham, NC, USA.

<sup>17</sup>Duke Eye Center, Center for Retinal Degenerations and Ophthalmic Genetic Diseases and Visual Function Diagnostic Laboratory, Durham, NC, USA.

<sup>18</sup>Translational Medicine, UCB Pharma, Slough, UK.

<sup>19</sup>Unit of Muscular and Neurodegenerative Diseases, Department of Neurosciences, Bambino Gesù Children's Hospital, IRCCS, Rome, Italy.

<sup>20</sup>Department of Pediatric Subspecialties, Division of Nephrology – Bambino Gesù Children's Hospital, Rome, Italy.

<sup>21</sup>Department of Laboratories - Pathology Unit Bambino Gesù Children's Hospital, Rome, Italy.

<sup>22</sup>Department of Pharmacy and Biotechnology (FABIT), University of Bologna, Bologna, Italy.

<sup>23</sup>Translational Medicine, UCB Pharma, Braine-l'Alleud, Belgium.

<sup>24</sup>Department of Neurology, Medical University Innsbruck, Austria.

<sup>25</sup>Department of Pediatrics, Salzburger Landeskliniken and Paracelsus Medical University Salzburg, Salzburg, Austria.

<sup>26</sup>Department of Medical and Surgical Sciences, University of Bologna, Italy.

<sup>27</sup>Stanley Manne Children's Research Institute, Ann & Robert H. Lurie Children's Hospital of Chicago, Chicago, IL, USA

<sup>28</sup>Departments of Pediatrics and Cellular and Molecular Biology, Northwestern University Feinberg School of Medicine, Chicago, IL, USA

\*Shared co-first authors

#Shared co-senior authors

&Corresponding authors:

Tommaso Pippucci, Medical Genetics Unit, Sant'Orsola-Malpighi University Hospital, via Massarenti 9, 40138 Bologna, Italy. Phone: +39.0512088421.; Email: [tommaso.pippucci@unibo.it](mailto:tommaso.pippucci@unibo.it).  
Valerio Carelli, IRCCS Istituto delle Scienze Neurologiche di Bologna, UOC Clinica Neurologica, via Altura 3, 40139, Bologna, Italy. Phone: +39.0514966747; Email: [valerio.carelli@unibo.it](mailto:valerio.carelli@unibo.it).

The authors have declared that no conflict of interest exists.

## 1 **Abstract**

2 Inherited optic neuropathies include complex phenotypes, mostly driven by mitochondrial  
3 dysfunction. We report an optic atrophy spectrum disorder, including retinal macular dystrophy and  
4 kidney insufficiency leading to transplantation, associated with mitochondrial DNA (mtDNA)  
5 depletion without accumulation of multiple deletions. By whole-exome sequencing, we identified  
6 mutations affecting the mitochondrial single strand binding protein (SSBP1) in four families with  
7 dominant and one with recessive inheritance. We show that *SSBP1* mutations in patient-derived  
8 fibroblasts variably affect its amount and alter multimer formation, but not the binding to ssDNA.  
9 *SSBP1* mutations impaired mtDNA, nucleoids and 7S-DNA amounts as well as mtDNA replication,  
10 impacting replisome machinery. The variable mtDNA depletion in cells reflected in severity of  
11 mitochondrial dysfunction, including respiratory efficiency, OXPHOS subunits and complexes  
12 amount and assembly. mtDNA depletion and cytochrome c oxidase-negative cells were found *ex-*  
13 *vivo* in biopsies of affected tissues, like kidney and skeletal muscle. Reduced efficiency of mtDNA  
14 replication was also reproduced *in vitro*, confirming the pathogenic mechanism. Furthermore, *ssbp1*  
15 suppression in zebrafish induced signs of nephropathy and reduced optic nerve size, the latter  
16 phenotype complemented by wild-type mRNA but not by *SSBP1* mutant transcripts. This  
17 previously unrecognized disease of mtDNA maintenance implicates *SSBP1* mutations as cause of  
18 human pathology.

## 19 **Introduction**

20 The expanding genetic landscape of inherited optic neuropathies has highlighted mitochondrial  
21 dysfunction as a major driver of this pathology (1, 2). Overall, the genetic defects leading to optic  
22 atrophy range from mitochondrial DNA (mtDNA) point mutations in Leber's hereditary optic  
23 neuropathy (LHON) (3), to dominant and recessive mutations affecting a cluster of nuclear genes  
24 implicated in mitochondrial dynamics (4). These include *OPA1*, whose protein product is necessary  
25 for fusing the inner mitochondrial membrane (5, 6), *MFN2* for fusion of the outer mitochondrial  
26 membrane (7), *DNM1L* (8), *OPA3* (9) and *SLC25A46* (10) involved in mitochondrial fission. In  
27 addition to optic neuropathy, mutations in several of these genes have also been hallmarked by  
28 broader clinical phenotypes defined as "plus", associated with mtDNA instability, as characterized  
29 by secondary accumulation of multiple deletions in post-mitotic tissues such as skeletal muscle and  
30 brain (11, 12, 13). In patients, mtDNA multiple deletions are phenotypically reflected by ocular  
31 myopathy with chronic progressive external ophthalmoplegia (CPEO) and ptosis, in association or  
32 not with more widespread brain involvement, including parkinsonism and dementia (14, 15).  
33 Originally, CPEO and ptosis with mtDNA multiple deletions were noted for their remarkable  
34 association of Mendelian inheritance and secondary mtDNA instability (16). The genes associated  
35 with this initial group of mitochondrial disorders were all implicated in mitochondrial replisome,  
36 such as the mitochondrial polymerase (*POLG1* and *POLG2*), the helicase Twinkle (*TWNK*), other  
37 genes instrumental to mtDNA replication (*RRM2B*, *RNaseH1*, *DNA2*, *MGME1*), and genes  
38 implicated in nucleotide availability and balance (*SLC25A4*, *TYMP*, *TK2*, *DGOUK*, *MPV17*) (17).  
39 We are now aware that allelic mutations in all these genes, respectively implicated in mitochondrial  
40 dynamics, replisome and nucleotide metabolism, may either affect so profoundly mtDNA  
41 replication that the major outcome is depletion of mitogenomes with fatal infantile  
42 encephalomyopathies, or induce slow somatic accumulation of mtDNA multiple deletions with  
43 various syndromes of adult life dominated by CPEO (18).

44 However, one key factor implicated in mtDNA replication has been missing: the mitochondrial  
45 single strand binding protein SSBP1, cloned in 1993 (19) and mapped to 7q34 in 1995 (20). Despite  
46 being a good candidate for mtDNA maintenance disorders, it was not pathogenically associated to  
47 any human disease. SSBP1 has been shown to coat the displaced, parental H-strand during mtDNA  
48 synthesis, a critical function according to the strand displacement mode of mtDNA replication (21).  
49 Here, we report the identification of a spectrum of phenotypes associated with *SSBP1* mutations and  
50 mtDNA depletion transmitted as autosomal dominant and recessive traits, which ranged from  
51 isolated optic atrophy to additional clinical features including retinal macular dystrophy,  
52 sensorineural deafness, mitochondrial myopathy, and kidney failure necessitating transplantation.

53

## 54 **Results**

### 55 **Exome sequencing identifies dominant and recessive mutations in *SSBP1***

56 *SSBP1* mutations and their segregation in five unrelated families. Two unrelated families from Italy  
57 and the US with the common feature of congenital or early onset optic atrophy, negative for the  
58 most frequent causes, underwent trio whole exome sequencing (WES) independently in different  
59 centers (Supplemental Material, Supplemental Table 1).

60 *De novo* mutations in *SSBP1* were identified in both families, which we connected through  
61 GeneMatcher (22). In the Italian family (Family 1 in Figure 1), we identified a heterozygous  
62 missense mutation NM 003143.2: c.320G>A (p.R107Q) (Supplemental Table 2), which arose *de*  
63 *novo* in the father and was transmitted to his affected child. The US proband (Family 2 in Figure 1)  
64 carried a *de novo* heterozygous missense mutation c.119G>T (p.G40V) (Supplemental Table 2).

65 Based on these findings, a total of 135 Italian probands with optic atrophy of unknown genetic  
66 origin was screened for *SSBP1* mutations. In two unrelated individuals, we found additional  
67 heterozygous missense mutations in *SSBP1*: c.331G>C (p.E111Q) in Family 3 and c.184A>G  
68 (p.N62D) in Family 4 (Figure 1; Supplemental Table 2). No members of Family 3 were available  
69 for segregation. In Family 4, the heterozygous mutation segregated in both proband's offspring,

70 whereas it was absent in his mother (the only parent available for testing). The father died in his  
71 70s, without any report of visual impairment. The segregation was therefore compatible with a *de*  
72 *novo* event in the proband.

73 In a fifth family from Austria, with a single proband (Family 5; Figure 1) presenting with a largely  
74 overlapping phenotype, WES identified a homozygous mutation in *SSBPI*, c.394A>G (p.I132V)  
75 (Supplemental Table 2). Parental consanguinity was not reported, and estimation of genomic  
76 inbreeding using WES data failed to reveal excess of homozygosity (Supplemental Table 3).  
77 Homozygosity for p.I132V can be explained as a founder mutation because the parents are from a  
78 remote mountain area in Austria.

79 *Clinical presentation of affected individuals.* Family 1 included two probands, a father and son, who  
80 presented with childhood onset optic atrophy, retinal macular dystrophy, sensorineural deafness and  
81 nephropathy, which in the child ultimately led to kidney transplantation (Figure 2 A-C;  
82 Supplemental Figure 1; Supplemental Case reports). Muscle and kidney biopsies from both patients  
83 revealed histoenzymatic features compatible with mitochondrial dysfunction, such as cytochrome c  
84 oxidase (COX) negative cells (Figure 2, B and C and Supplemental Figure 1B). The mtDNA  
85 molecular analysis revealed partial depletion of copy number in both tissues (Figure 2, D and E).  
86 Blood-derived cells were also mtDNA depleted, similar to kidney and muscle (Figure 2F).  
87 However, both long range and digital droplet PCR failed to identify and quantify mtDNA-deleted  
88 molecules in kidney, muscle, blood and urinary sediment cells (Supplemental Figure 2, A-D). A  
89 slight reduction of 7S DNA, the third strand of the mtDNA displacement loop (D-loop) was also  
90 noted (Supplemental Figure 2, E-H). Thus, muscle and kidney histoenzymatic analysis, as well as  
91 mtDNA investigations, were suggestive of mitochondrial dysfunction as pathogenic mechanism.  
92 Family 2 included a single proband presenting a similar phenotype, with childhood-onset severe  
93 optic atrophy and progressive retinal degeneration exhibiting a cone-rod dystrophy (CORD)  
94 phenotype (Figure 3). Despite relatively good foveal preservation, visual acuity was severely  
95 reduced due to the severity of the optic atrophy. In association to these eye findings, this patient

96 also exhibited progressive nephropathy requiring transplantation and sensorineural hearing loss. No  
97 functional or histological studies were available for this patient.

98 The sporadic patient of Family 3 was in his 70s and presented with isolated optic atrophy and no  
99 retinal changes in the macula. The proband of Family 4 had two affected offspring with neuro-  
100 ophthalmological assessment revealing features virtually identical to Family 1 in all three  
101 individuals (Figure 2A). The mtDNA analysis in blood-derived cells of patients from Family 3 and  
102 4 revealed a copy number in the lower end of the control range, suggesting a tendency to reduction  
103 (Supplemental Figure 2J).

104 The proband of Family 5, with homozygous p.I132V, initially developed blindness due to retinal  
105 dystrophy, and deafness. This clinical picture was later complicated by hypertrophic  
106 cardiomyopathy, nephropathy, ataxia and growth retardation. Muscle biopsy revealed COX  
107 negative fibers; biochemical studies documented a combined deficiency of complex I and III  
108 whereas citrate synthase was elevated.

109 *SSBP1 mutations frequency and in silico prediction of deleteriousness.* All dominant mutations  
110 were novel based on the variant database gnomAD v2.0.2. The recessive mutation was reported in  
111 only two heterozygous alleles in gnomAD, absent in the homozygous state. All missense mutations  
112 were evolutionarily conserved (phyloP100way scores ranging 6.2-8.9), with high potential for  
113 deleteriousness according to Combined Annotation Dependent Depletion (CADD Phred scores  
114 ranging 21.8-29.4) (Supplemental Table 2). All mutations mapped within the Single Strand Binding  
115 Domain (Figure 4A) and two of them (p.R107Q and p.E111Q) affected residues under the strongest  
116 purifying selection relative to SSBP1 according to Missense Tolerance Ratio (MTR), having MTRs  
117 within the 5<sup>th</sup> percentile of most missense depleted regions of the gene (Figure 4B). Mutations  
118 p.G40V, p.R107Q, and p.E111Q are predicted to disrupt molecular function according to *in silico*  
119 protein structure modeling by VIPUR (Supplemental Material, Supplemental Table 4) (23),  
120 although with seemingly distinct deleterious effects (Figure 4C). The p.G40V is predicted to have  
121 an unfavorable backbone conformation and appears to disrupt the interaction of SSBP1 with ssDNA

122 by destabilizing the nearby nucleotide-binding residues. Conversely, p.E111Q and p.R107Q are  
123 predicted to impact SSBP1 oligomerization by disruption of stabilizing salt-bridges of E111 and  
124 R107 with H34 and E27, respectively. Both p.N62D and p.I132V are not predicted to be grossly  
125 disruptive. However, p.N62D occurs at dimer interface, in close spatial proximity to R107, and  
126 introduces a negative charge that may interfere with dimerization. Finally, p.I132V is assumed to be  
127 tolerated mainly due to incomplete site conservation, however it still has a high structural disruption  
128 score that suggests destabilizing potential. Notably, all three mutations with a disruptive prediction  
129 appear to act through distinct mechanisms: p.G40V damaging ssDNA binding, p.R111Q disrupting  
130 tetramer assembly, and p.R107Q disrupting both dimerization and tetramerization.

131

### 132 **Analysis of SSBP1 protein in patient-derived mutant fibroblasts**

133 To assess the functional impact of *SSBP1* mutations on protein level, we performed Western blot  
134 analysis on mitochondria isolated from primary fibroblasts of four patients (both patients from  
135 Family 1, probands from Families 2 and 5) and from controls. Quantification of SSBP1 relative to  
136 the loading control VDAC1 indicated that abundance of p.R107Q mutant was comparable to  
137 controls, while p.G40V showed a significantly increased level of about 25 %, and p.I132V mutant a  
138 significant decrease of 39 % protein level instead (Figure 5, A and B). Immunofluorescence  
139 experiments evaluating co-localization of SSBP1 with MitoTracker red, revealed a trend, congruent  
140 with Western blot analysis, towards an increase in the mutant p.G40V protein and decrease in the  
141 p.I132V (Figure 5, C and D).

142 To monitor the effects of the mutations on homo-oligomerization of SSBP1, we performed a protein  
143 cross-linking experiment with isolated mitochondria treated with 0.1% glutaraldehyde (GA) to  
144 induce protein cross-linking, or untreated. Lysates were then separated on a denaturing SDS-  
145 polyacrylamide gel and the SSBP1 monomer, dimer, trimer and multimer were detected by Western  
146 blot. In the absence of GA (-) the majority of the SSBP1 protein was in the monomeric form  
147 (molecular weight ~15kDa), whereas in the presence of GA (+) some SSBP1 oligomers were cross-

148 linked (Figure 5E). The relative levels of the oligomeric cross-linked products (GA<sup>+</sup>) and the  
149 monomeric form (GA<sup>-</sup>) were determined by densitometry and expressed as a ratio, where the ratio  
150 for controls was set equal to 1 (Figure 5F). The p.R107Q and p.G40V mutations induced the  
151 accumulation of dimeric and trimeric forms, while the detection of SSBP1 tetramers and multimers  
152 was severely reduced in the case of p.R107Q, but not affected by p.G40V. In the cell line with  
153 p.I132V mutation we hardly detected any trimeric and multimeric products. These results suggest  
154 that p.R107Q and p.I132V mutations interfere with SSBP1 multimerisation.

155 Next, we tested binding of wild-type (wt) and affected proteins to ssDNA. We performed an *in vitro*  
156 pull-down assay by incubating mitochondrial lysate with biotinylated ssDNA. We found that the  
157 SSBP1 antibody detected the protein only in the pull-down fraction both in controls and patients  
158 (Figure 5G). No protein was observed in the supernatant, indicating that wt and *SSBP1* mutants  
159 were able to bind ssDNA. Moreover, anti-HSP60, anti-VDAC and anti-ETHE1 antibodies were  
160 able to detect the corresponding proteins exclusively in the supernatant but not in the pull-down  
161 fraction. These results indicated that only the SSBP1-ssDNA complex was precipitated specifically.  
162 Since we were wondering how the complex SSBP1(p.I132V mutation)-ssDNA could be  
163 precipitated despite only small amounts of tetramers were detected, we expressed the mutant protein  
164 in *E. coli* and tested its ability to form tetramers. Size exclusion chromatography of wt and p.I132V  
165 mutation demonstrated in both cases a stable tetramer (Supplemental Figure 3A). However, as  
166 observed by differential scanning fluorimetry, the p.I132V mutation has a somewhat lower  
167 thermostability than wt SSBP1, indicative of mild alterations to the physical properties of the  
168 mutation, though both proteins melt well above physiologically relevant temperatures  
169 (Supplemental Figure 3B). Together, these experiments suggest that the different mutations did not  
170 prevent binding of the SSBP1 protein to ssDNA under these experimental conditions.

171

172 **Analysis of mutant fibroblasts reveals depletion of mtDNA and nucleoids with altered**  
173 **dynamics of mitogenomes repopulation and impaired *in vitro* replication**

174 Based on the partial mtDNA depletion observed in patient-derived tissues (Figure 2, D-F), we  
175 investigated mtDNA maintenance in *SSBP1* mutant fibroblasts by quantifying nucleoid and mtDNA  
176 copy numbers compared to controls. In all four patient cell lines we found significantly reduced  
177 mtDNA content, ranging from 54% to 78% depletion compared to controls (Figure 6A). The  
178 p.I132V mutation appeared the less severe in terms of mtDNA depletion, whereas p.R107Q II and  
179 p.G40V were the most severe (Figure 6A). This result was matched by nucleoid quantification, as  
180 assessed by PicoGreen/MitoTracker red combined staining, showing a significant reduction of  
181 nucleoids, particularly prominent in p.R107Q II and p.G40V cells (Figure 6, B and C).

182 To assess the global efficiency of mtDNA replication, we next performed a depletion/repopulation  
183 experiment, in which cells were mtDNA depleted by seven days exposure to low concentration of  
184 Ethidium Bromide (EtBr), followed by its withdrawal and mtDNA repopulation in 15 days. Each  
185 mutant cell line started from a lower mtDNA content at point 0, reached a profound depletion  
186 similar to controls at day seven, and resumed mtDNA replication with different efficiencies (Figure  
187 6D). The most severe effects were observed for p.R107Q and p.G40V mutations, whereas the  
188 homozygous p.I132V mutation was associated with milder outcome. Considering the mtDNA  
189 amount at point 0 as 100 %, it is notable that only p.R107Q was significantly slower in  
190 mitogenomes repopulation (Supplemental Figure 4A). At the last time point of this experiment all  
191 cell lines approximately regained the original levels of mtDNA copy number, with the exception of  
192 R107Q I.

193 The same samples were also quantified for 7S DNA (Figure 6E). Control fibroblasts at time 0 had  
194 ratio of 7S DNA/mtDNA of ~0.43. This ratio matched perfectly the changes of mtDNA copy  
195 number during the EtBr experiment in controls, with a similar pattern for the mild p.I132V mutation  
196 (ratio 0.28 at time 0). In contrast, p.R107Q and p.G40V mutations showed a low amount of 7S  
197 DNA (0,09 and 0.03 at time 0, respectively), which remained mostly unchanged during the  
198 experiment. No deletions were observed at time 0 and 15 (data not shown).

199 To assess the possible presence of low levels of mtDNA heteroplasmic mutations, which might  
200 expand after the depletion/repopulation experiment, mtDNA deep sequencing (mean coverage  
201 7412X) was carried out at point 0 and at 15 days post-EtBr withdrawal. Overall, mutant cells at  
202 time 0 had a significantly higher number of heteroplasmic variants, considering heteroplasmy  
203 within 20 % of total copy number, but the load of heteroplasmy did not differ compared to controls,  
204 and was not substantially changed by the bottleneck due to EtBr treatment at day 15 (Supplemental  
205 Figure 4, B-E). The mtDNA complete sequence of all cell lines, and blood circulating cells for the  
206 remaining cases, allowed for reconstruction of the haplotype of each individual enrolled in this  
207 study and their phylogenetic relationship (Supplemental Excel file). The only notable variant was  
208 observed in the case R107Q II (Pt 2 in Family 1), who presented a novel C insertion at position 57  
209 (57insC) within the OH region.

210 Next, we quantified the levels of TFAM and other components of the mtDNA replisome (Figure 6,  
211 F and G). Western blot analysis revealed a significant reduction of TFAM, RNaseH1 and  
212 TWINKLE in both p.R107Q mutant cells, with only a modest decrease of POL $\gamma$ . In contrast, we did  
213 not observe any protein reduction in the other two mutant cell lines with a significant increase of  
214 POL $\gamma$  in p.G40V mutant. Overall, these results suggest a severe effect of p.R107Q and p.G40V  
215 mutations on mtDNA maintenance, replication and 7S DNA amount in fibroblasts. The p.I132V  
216 mutation was associated with only a baseline mtDNA reduction, confirming its milder nature.

217 SSBP1 is known to stimulate the activity of POL $\gamma$  (24), thus we decided to investigate *in vitro* if the  
218 identified mutations affected this ability. To this end, we purified wt SSBP1 and mutant derivatives  
219 thereof in recombinant form and analyzed them on SDS-PAGE to confirm purity (Figure 7A). We  
220 next monitored the ability of SSBP1 to stimulate DNA synthesis on a circular, ssDNA template of  
221 about 3000 nt in the presence of POL $\gamma$ . The primer needed to initiate DNA synthesis was a <sup>32</sup>P-  
222 labeled oligonucleotide (50 nt) that had been annealed to ssDNA substrate. We used saturating  
223 amounts of SSBP1 that could cover the single-stranded template completely (one SSBP1 tetramer  
224 was calculated to bind 60 nt ssDNA). All mutations were able to support full-length DNA synthesis

225 (Figure 7B, compare lanes 1-5, no SSBP1 added, with 11-35), but were all less efficient than the wt  
226 protein (Figure 7B, lanes 6-10). In conclusion, all SSBP1 mutations had reduced ability to stimulate  
227 POL $\gamma$ -dependent DNA synthesis *in vitro*.

228

### 229 **mtDNA depletion reflects on bioenergetics of *SSBP1* mutant fibroblasts**

230 Considering the mtDNA depletion in all patient fibroblasts, we next characterized the impact of  
231 *SSBP1* mutations on bioenergetics. Oxygen consumption rate (OCR) analysis showed a severe  
232 respiratory deficit in both p.R107Q mutant cells, a partial defect in p.G40V, whereas no differences  
233 were found for p.I132V mutation (Figure 8, A and B). Furthermore, all mutants, with the exception  
234 of p.I132V, showed a significant shift toward glycolysis, as indicated by decreased OCR/ECAR  
235 ratio (Supplemental Figure 4F).

236 We also performed Western blot analysis of representative subunits of OXPHOS complexes (Figure  
237 8, C and D). A marked decrease in the amount of NDUFB8 and NDUFA9 (CI), and COX II (CIV)  
238 characterized p.R107Q cells, with a slight reduction of UQCRC2 (CIII), statistically significant  
239 only in R107Q-II. The p.G40V mutation was associated with a milder but significant reduction of  
240 CI subunits and an increase of UQCRC2. Concordant with OCR result, p.I132V cells did not show  
241 reduction of OXPHOS subunits, but rather an increase of UQCRC2 and COX II. To confirm these  
242 data, we quantified the amount of assembled complexes by Blue-Native page (Figure 8E). All  
243 patient cell lines, with the exception of p.I132V, exhibited a significant reduction of CI, both by  
244 western blot and in-gel activity (Figure 8F), and a partially disassembled CV, as shown by the  
245 appearance of two bands at lower molecular weight corresponding to free F1 (Figure 8G). No  
246 alteration of CIII amount was observed (Figure 8F). Finally, the analysis of supercomplexes  
247 assembly showed similar results, with reduction of supercomplexes containing complex I (I+III<sub>2</sub>,  
248 I+III<sub>2</sub>+IV and I+III<sub>2</sub>+IV<sub>n</sub>), and increase of isolated CIII<sub>2</sub>, not assembled with CI, in fibroblasts  
249 carrying p.R107Q and p.G40V mutations. Again, the incomplete assembly of CV has been detected  
250 in these three cell lines (Supplemental Figure 4G).

251 To assess if mtDNA depletion was paralleled by a reduction of mitochondrial mass, we quantified  
252 citrate synthase (CS), TIM23 and TOM20 levels (Figure 8, H and I). This analysis revealed a slight  
253 reduction and an increase of mitochondrial mass in R107Q-II and G40V mutations, respectively.  
254 These results indicate that the SSBP mutations p.R107Q and p.G40V cause an energetic defect  
255 driven by CI reduction, a defect that was less severe in the latter mutation, probably due to the  
256 compensatory increment of mitochondrial mass. In contrast, fibroblasts carrying p.I132V, despite  
257 having mtDNA depletion, did not display a detectable energetic defect.

258 To evaluate if the phenotypic defect due to the homozygous recessive mutation could be rescued by  
259 the wild-type protein, we integrated by lentiviral transduction the wild-type SSBP1 in a control and  
260 in the p.I132V cell lines. The SSBP1 complementation, confirmed by Western blot (Supplemental  
261 Figure 5, A and B), rescued the mtDNA copy number and induced a non-significant increase in  
262 respiration in p.I132V cells (Supplemental Figure 5, C-E).

263

#### 264 **Disruption of *ssbp1* in zebrafish results in optic nerve atrophy and mitochondrial depletion**

265 *SSBP1* has an established role in mitochondrial biogenesis and previous RNA *in situ* hybridization  
266 studies have documented ubiquitous expression in zebrafish from 0-2.5 days post fertilization (dpf)  
267 (25). To establish relevance of *SSBP1* disruption to the optic atrophy phenotype of patients, we  
268 generated zebrafish models. We performed reciprocal BLAST searches and identified a single  
269 ortholog in the zebrafish genome (72 % identity; 87 % similarity for human [NP\_003134.1] vs.  
270 zebrafish [NP\_001017806.1] protein). Next, we generated and characterized an efficient single  
271 guide (sg)RNA targeting *ssbp1* exon 4 (Supplemental Figure 6A); we injected 50 pg sgRNA with  
272 100 pg of Cas9 protein into one cell stage embryos, performed heteroduplex analysis, and estimated  
273 an average mosaicism of ~94 % in F0 mutant embryos (Supplemental Figure 6, B and C). At 2 dpf,  
274 F0 *ssbp1* mutants displayed no overt morphological abnormalities compared to controls  
275 (Supplemental Figure 6D).

276 We and others have reported previously that the zebrafish is a tractable model for evaluating optic  
277 nerve ultrastructure (26, 27). To assess optic nerve integrity, we conducted immunostaining of  
278 whole mount F0 mutant embryos fixed at 2 dpf and stained with anti-acetylated tubulin antibody  
279 (investigator masked to experimental condition). We acquired ventral images of whole mount  
280 embryos using fluorescence microscopy, and measured the area of the optic nerve chiasm at a  
281 consistent position framed bilaterally by the notochord (Figure 9A; Supplemental Figure 6E). We  
282 found that F0 mutants display an optic nerve phenotype indistinguishable from uninjected controls  
283 or batches injected with an equivalent dose of sgRNA alone (Supplemental Figure 6, E and F).  
284 Additionally, we performed qRT-PCR on RNA harvested from F0 *ssbp1* embryos at 2 dpf  
285 (Supplemental Figure 6G), but consistent with our optic nerve phenotyping data, we did not find  
286 any significant differences between mutants versus controls.

287 We hypothesized that the apparent lack of early optic nerve phenotype in F0 mutants could be due  
288 to the presence of maternal *ssbp1*, and we aged animals for evaluation at later time points. By three  
289 weeks post fertilization, we saw marked growth restriction and lethality in F0 larvae compared to  
290 controls. We speculated that the F0 mutant lethality could be due to the depletion of mitochondria  
291 over time. To explore this possibility, we injected 50 pg sgRNA plus 100 pg Cas9 protein into the  
292 *Tg(XIEef1a1:mlsEGFP)* transgenic zebrafish line, which targets GFP to the mitochondria with the  
293 COXVIII mitochondrial localization signal (mls). We aged F0 mutants to 15 dpf, obtained lateral  
294 fluorescent images, and quantified GFP intensity in the lens of live anesthetized embryos.

295 Consistent with our hypothesis, we found a significant reduction of green signal in F0 mutants  
296 compared to controls or larvae injected with sgRNA alone (Supplemental Figure 6, H and I).

297 We next sought to evaluate the effects of *ssbp1* loss at an earlier developmental time point by using  
298 a translation blocking (tb) morpholino (MO) to suppress *ssbp1* transcript (both maternal and  
299 embryonic mRNA; Supplemental Figure 7A). To determine the efficiency of *ssbp1* tb MO, we  
300 performed immunoblotting on total protein extracted from pools of embryos at 2 dpf; we observed  
301 depletion of *ssbp1* protein in morphants reduced to ~5% of protein levels in controls (Supplemental

302 Figure 7, B and C). Next, we tested a dose curve by injecting tb-MO in one to four cell stage  
303 embryos at three different doses (1 ng, 2 ng and 3 ng). Immunostaining and quantification of optic  
304 nerve chiasm area at 2 dpf showed a dose-dependent and significant reduction in optic nerve size  
305 for each dose tested in comparison to controls (Supplemental Figure 7, D and E). To determine the  
306 specificity of the tb-MO phenotype, we co-injected wt human *SSBPI* mRNA with MO and  
307 observed a significant amelioration of the optic nerve phenotype to a level nearly indistinguishable  
308 from controls (Figure 9, A-C; Supplemental Figure 8, A and B). We also matured larvae to 4 dpf, a  
309 developmental time point by which the zebrafish pronephros is formed (28,29). We noted a dose-  
310 dependent cardiac, yolk sac, and peri-orbital edema suggestive of nephropathy (30) (Supplemental  
311 Figure 7, F and G). However, other phenotypes, such as abnormal otolith formation (a proxy for the  
312 mammalian ear) relevant to our *SSBPI* human cohort were indistinguishable in *ssbpl* morphants  
313 versus controls (Supplemental Figure 9A). Additionally, we did not detect differences in mlsEGFP  
314 quantity in morphants on our mitochondrial transgenic reporter at 2 dpf, possibly due to detection  
315 thresholds at this early developmental stage (Supplemental Figure 9, A and B). Finally, we  
316 quantified mtDNA content in *ssbpl* morphants and controls using a qPCR assay to monitor mtDNA  
317 amount relative to nuclear DNA (using *mt-nd1* and *polg1* primers, respectively; 2 dpf embryo pools  
318 of 30 embryos each), and did not detect significant differences between either experimental group  
319 (Supplemental Figure 9C).

320 *In vivo* complementation is a sensitive and specific approach to test pathogenicity of  
321 nonsynonymous mutations in the context of optic nerve phenotypes (26). To test the effect of the  
322 missense mutations identified in affected individuals (including those studied in fibroblasts as well  
323 as the other two mutations found in Family 3 and 4), we co-injected MO with *SSBPI* mutation-  
324 bearing mRNAs and compared their rescue efficiency with that of wt *SSBPI* message or MO alone.  
325 For each of the p.G40V, p.N62D, p.R107Q, p.E111Q and p.I132V encoding mRNAs, we detected  
326 no significant difference between MO alone and mutant mRNA rescue experiments, suggesting that  
327 they are functional null mutations (Figure 9, A-C; Supplemental Figure 8, A and B). Consistent

328 with the *in vitro* studies, we observed a milder effect for p.I132V, the sole mutation that segregated  
329 in a recessive inheritance pattern. Although p.I132V mRNA rescued optic nerve chiasm area less  
330 efficiently than wt mRNA, the mean optic nerve area was improved by 18% in p.I132V rescue  
331 batches compared to MO alone ( $p=0.0148$ , two-tailed unpaired t-test). However, this difference did  
332 not reach statistical significance when corrected for multiple testing (Figure 9, A-C; Supplemental  
333 Figure 8, A and B). Further, *SSBPI* complementation with mRNA harboring a common variant  
334 (p.L75P: 5 homozygotes in gnomAD; MAF  $1.776e-3$ ) rescued similarly to wt mRNA, supporting  
335 the specificity of our assay (Figure 9, A-C; Supplemental Figure 8, A and B). Injection of mRNA  
336 encoding any of the five patients' mutations, p.L75P, or wt *SSBPI* yielded no apparent optic nerve  
337 phenotype compared with controls (Figure 9D; Supplemental Figure 8C). Moreover, titration of wt  
338 and p.R107Q mRNAs did not show any significant phenotype (Supplemental Figure 8D),  
339 suggesting that dominant-negative effect of these mutations is unlikely.

340 Together, our data indicate that MO-based zebrafish models of *ssbpl* suppression recapitulate optic  
341 nerve atrophy observed in individuals with dominant and recessive *SSBPI* mutations. Furthermore,  
342 our *in vivo* complementation data suggest that missense mutations in cases confer a loss of function,  
343 supporting a loss of function model of disease when cellular levels of mitochondria fall below a  
344 critical dosage threshold.

## 345 **Discussion**

346 We report *SSBPI* mutations associated with an optic atrophy spectrum disorder including retinal  
347 dystrophy, kidney insufficiency requiring transplantation, sensorineural deafness and mitochondrial  
348 myopathy with mtDNA depletion. *SSBPI* mutations impaired mtDNA maintenance and replication,  
349 as demonstrated in cells and *in vitro*. Reduced mtDNA copies reflected in a variable phenotype of  
350 impaired OXPHOS, either *in vitro* studying fibroblasts or *ex vivo* in biopsies of affected tissues, like  
351 kidney and skeletal muscle. In zebrafish, loss of *ssbp1* was shown to affect optic nerve development  
352 and induce signs of nephropathy. All mutants failed to rescue the optic nerve phenotype, suggesting  
353 that dominant mutations induced loss of function, whereas the recessive behaved as a hypomorph.  
354 From the genotype-phenotype standpoint a few features deserve a comment. To date, almost all  
355 mtDNA depletion disorders are fatal infantile syndromes (17), whereas we describe an adult disease  
356 dominated by optic atrophy with pure partial mtDNA depletion, without coexisting multiple  
357 deletions. A further example of adult phenotype with prevalent mtDNA depletion is the spectrum  
358 disorder associated with recessive mutations in *MPV17*, ranging from severe epatho-cerebral  
359 encephalopathy to adult neuro-hepatothopathy, recurrent in Navajo Indians (31, 32). Differently,  
360 mitochondrial neuro-gastro-intestinal-encephalopathy (MNGIE), another adult disease with mtDNA  
361 depletion, combines also multiple deletions and CPEO/ptosis (33). Remarkably, none of our  
362 patients displayed CPEO or ptosis, which is usually the hallmark of mtDNA multiple deletions  
363 accumulation, such as in MNGIE and DOA “plus” phenotypes (11,12,14,15,17), or of sporadic  
364 mtDNA single deletion, such as in Kearns-Sayre syndrome (KSS) (34). Thus, these *SSBPI*  
365 mutations selectively impinge on efficiency of mtDNA replication, apparently without affecting its  
366 fidelity. Interestingly, optic atrophy most probably is a congenital or childhood-onset reduction of  
367 axons that remains stable in adulthood, frequently combined with a prevailing cone retinal  
368 degenerative phenotype that worsens over time. Most patients exhibited a foveal cone photoreceptor  
369 ellipsoid zone (EZ) loss, visible as a foveal hyporeflective gap of EZ and retinal pigmented  
370 epithelium (RPE) layers (Figure 2A). This resembles the known cavitation lesions seen in

371 congenital disorders such as achromatopsia (35, 36) and blue cone monochromacy (37), as well as  
372 in degenerative entities such as KCNV2-related retinopathy (38). A progressive cone-predominant  
373 disease expression configuring a CORD phenotype was seen in the Family 2 (p.G40V) proband,  
374 lacking the foveal cavitation but with a unique hyperreflectivity that persisted also as the retinal  
375 disease progressed. These neuro-retinal features have not been previously reported in mtDNA  
376 depletion syndromes, although a CORD phenotype is found in KSS (34), whereas the kidney  
377 involvement was observed since the first study on infantile syndromes with mtDNA depletion (39).  
378 Besides the genotype-phenotype variability with different *SSBP1* mutations, a different severity  
379 was also observed within Family 1 (p.R107Q). Dominant disorders frequently display incomplete  
380 penetrance, which may also reflect on phenotype expressivity. Nuclear background may obviously  
381 play a role, as well as mtDNA haplotype. Our complete mtDNA sequence only revealed an  
382 insertion affecting the OH region in the younger proband with severe nephropathy. This could  
383 affect mtDNA replication efficiency, potentially worsening the defect due to the *SSBP1* mutation.  
384 Specific experiments should be designed to confirm this hypothesis.

385 We documented causal association of *SSBP1* mutations with the disease, demonstrating, both *in*  
386 *vivo* and *in vitro*, that all patients' missense *SSBP1* mutations are pathogenic.

387 First, suppression of *ssbp1* transcript in zebrafish induced reduction of optic nerve chiasm size and  
388 depletion of mitochondria numbers, possibly affecting also kidney function. The optic nerve  
389 phenotype, the constant clinical feature in all patients, was fully rescued by wt or by the common  
390 polymorphism p.L75P mRNA, but not by mutant *SSBP1* mRNA, confirming their deleteriousness.  
391 These experiments clearly support loss of function for all dominant mutations, whereas the  
392 recessive mutation p.I132V, improving the optic nerve chiasm size less effectively as compared to  
393 wt, revealed its possible hypomorphic nature, which results in a disease outcome only when in  
394 homozygous state.

395 Second, cellular and *in vitro* studies clearly documented that all *SSBP1* mutations hamper mtDNA  
396 replication, as also evident by mtDNA copy number assessment in patient's tissues, including

397 skeletal muscle, kidney and blood. In fact, both depletion/repopulation experiment after EtBr in  
398 mutant fibroblasts and the *in vitro* synthesis experiment confirm that *SSBP1* mutations cause  
399 reduced efficiency of mtDNA replication. Indeed, the *in vitro* assay showed that even though the  
400 mutants could support full-length DNA synthesis, there was a delay as compared to the reactions  
401 with wt *SSBP1* indicating either lower affinity to the DNA or to the POL $\gamma$  holoenzyme. Regardless  
402 of the reason, the mutants seem to have lost some of their stimulatory effect, possibly giving a  
403 molecular explanation of the disease phenotype, i.e. decreasing the POL $\gamma$  activity.

404 Notably, all patients' mutations were missense changes, while we found no protein-truncating or  
405 splice-site alterations. This suggests that *SSBP1* dosage reduction is not the molecular mechanism  
406 underlying disease. Consistently, we did not observe reduction in protein products by Western blot,  
407 except for the recessive p.I132V. In large public population databases such as gnomAD, a few  
408 ultra-rare potential dosage-affecting *SSBP1* alleles (Supplemental Table 5) suggest that monoallelic  
409 haploinsufficiency may be tolerated or be implicated in overlapping disease phenotypes as possibly  
410 hypomorphic alleles. An example of this is the start-loss c.3G>A variant proposed to act as modifier  
411 for penetrance of the m.1555A>G mtDNA deafness mutation, associated with mtDNA depletion  
412 and multiple deletions limited to skeletal muscle (40).

413 *SSBP1* is a small protein and much of its surface is involved in binding interactions with DNA,  
414 itself and other replisome proteins. The pull-down experiments in fibroblasts failed to reveal a  
415 defect in ssDNA binding, also for the p.G40V, which was predicted to disrupt this interaction *in*  
416 *silico*. This apparent contradiction may be explained by the fact that pull-down experiment is not  
417 quantitative and cannot measure the dynamic of *SSBP1*–ssDNA interaction. Conversely, the cross-  
418 linking experiment showed that p.R107Q hampers *SSBP1* oligomerization, as predicted *in silico* for  
419 this mutation and its neighboring p.E111Q. Although p.N62D is predicted neutral, *in vivo* studies  
420 support it as a pathogenic mutation and its spatial proximity to p.R107Q suggests that the two  
421 mutations share the same mechanism. The recessive p.I132V was not predicted to be deleterious,  
422 however its destabilizing potential evidenced by lower thermostability, reduction of mutant *SSBP1*

423 oligomers, complementation studies in fibroblasts, and persistence of optic nerve atrophy in  
424 MO+p.I132V zebrafish, all argue in favor of its pathogenic potential.

425 Despite all mutant fibroblasts were characterized by decreased mtDNA amount, only p.R107Q cells  
426 presented a reduced TFAM level and replisome proteins, according to its most severe effect on  
427 mtDNA replication. Considering that TFAM stabilizes mtDNA by packing single mito-genome into  
428 nucleoids (41,42), we would have rather expected that all mutants displayed a similar trend of  
429 reduced TFAM level. Furthermore, we also observed a gradual worsening of mitochondrial  
430 energetic functions based on the different mutations: no energetic alteration on p.I132V, a partial  
431 respiratory defect driven by CI-reduction in p.G40V, and a very severe energetic deficit in  
432 p.R107Q. We can speculate either that this latter mutation severely affects the stability of the  
433 replication-proteins and consequently impacts bioenergetic efficiency, or that p.G40V and p.I132V  
434 cells may have particularly efficient compensatory activation of mitochondrial biogenesis. Our  
435 results support this last hypothesis. Indeed, we found that p.G40V fibroblasts presented an increase  
436 of mitochondrial mass, a mechanism observed also in other mitochondrial diseases, such as LHON  
437 (43). Remarkably, a mechanism of increased transcription efficiency in association with mtDNA  
438 depletion was already observed in the liver of Mpv17 knock-out mouse model (44). Thus, it is not  
439 surprising that these mutant cells had milder or no respiratory defect, also considering that  
440 fibroblasts are not the target tissue of the pathology and may display only a very mild energetic  
441 defect as previously reported (45,46). The SSBP1-associated disease, in fact, displayed a clear  
442 tissue-specificity in patients with an inconstant clinical expression in kidney, for example. Tissue-  
443 specific sensitivity to little variations in mtDNA depletion and compensatory response possibly  
444 determines the clinical expression. In the same line, the failure to detect a clear mtDNA depletion in  
445 2 dpf zebrafish embryos might just be due to the early stage at which this experiment was done and,  
446 again, to the tissue-specific reduction of mtDNA copy number.

447 SSBP1 is required for efficient initiation and elongation of mtDNA replication (47,48). A majority  
448 of all mtDNA replication events are prematurely terminated at the end of the D-loop, forming 7S

449 DNA. The relative levels of abortive mtDNA replication appear to be a regulated event. When more  
450 mtDNA is required, 7S DNA synthesis is reduced in favor of complete mtDNA replication (49,50).  
451 The drop in 7S DNA levels associated with mutations in mtSSB is therefore most likely a  
452 compensatory effect. Even if all three tested mutations (p.G40V, p.R107Q and p.I132V) negatively  
453 regulate mitochondrial genome stability, only dominant mutations induce a severe reduction of 7S  
454 abundance. The milder reduction of 7S DNA associated with p.I132V may be compatible with its  
455 hypomorphic nature. Alterations of 7S DNA levels have also been observed in other mitochondrial  
456 disorders caused by impaired mtDNA replication (51,52, 53).

457 In conclusion, we add *SSBPI* to the list of genes implicated in mtDNA maintenance human  
458 diseases. Our current findings will open many different avenues of further investigation, ultimately  
459 contributing to better understand mtDNA replication, enlarging the landscape of phenotypic  
460 expression of mitochondrial diseases in humans.

## 461 **Methods**

### 462 *Cells and culture conditions*

463 Skin fibroblasts were derived, after informed consent, from seven healthy donors, two related  
464 patients with the p.R107Q mutation, one patient with the p.G40V mutation and one patient with the  
465 p.I132V mutation. Fibroblasts were grown in DMEM medium supplemented with 10 % fetal bovine  
466 serum (FBS, Gibco, Life Technologies),  $2 \times 10^{-3}$  mol/L L-glutamine, 100 U/ml penicillin and 100  
467  $\mu$ g/ml streptomycin, in an incubator with a humidified atmosphere of 5 % CO<sub>2</sub> at 37 °C. The  
468 mtDNA depletion/repopulation experiment was performed as described (43). Briefly, cells were  
469 grown in glucose-medium supplemented 0.05mg/ml uridine and 50 ng/ml ethidium bromide (EtBr)  
470 to induce mtDNA depletion. After 7 days, EtBr was removed from the medium and cells were  
471 propagated until 15th day.

472

### 473 *mtDNA content and quantification of deletions and 7S DNA*

474 Quantification of mtDNA copy number relative to nuclear DNA (nDNA) was performed, for  
475 fibroblasts, muscle, kidney and blood tissues, as described (54).

476 Quantification of mtDNA deletion and 7S DNA was performed on fibroblasts, muscle, kidney,  
477 urine and blood tissues. Briefly, the absolute quantification of mitochondrial genome deletions is  
478 based on duplex amplification in droplet digital PCR (ddPCR) with specific probes in MT-ND4  
479 (major arc) and MT-ND1 (control region), adapted from published qPCR methods (55), and  
480 expressed as ratio ND4/ND1.

481 The quantification of 7S DNA was performed as previously described (51) and adapted to ddPCR  
482 (Bio-Rad). The 7S DNA is expressed as ratio -1 (mean  $\pm$  SD) of mtDNA+7S DNA over mtDNA  
483 using the primer pairs (a+b1) and (a+b2), respectively, where b1 is inside the 7S region, amplifying  
484 both mtDNA and 7S DNA, and b2 is outside, amplifying only mtDNA.

485

### 486 *Oligomerization assay*

487 SSBP1 oligomerization was carried out as described (56). Briefly, 10 µg of mitochondria isolated  
488 from controls and patients' primary fibroblasts as described (57) were treated or not with  
489 crosslinking agent (glutaraldehyde), final concentration 0.1 %. The reaction was quenched after 10  
490 min with  $100 \times 10^{-3}$  mol/L PBS/glycine. Monomers or multimers were detected by SDS-Page with  
491 anti-SSBP1 antibody. Densitometric analysis was carried out using ImageJ software, expressed as  
492 cross-linked oligomers to monomers ratio.

493

#### 494 ***Pull-down assay***

495 Pull-down assay was carried out as described (58, 59) with some modifications. Briefly, 10 µg of  
496 isolated mitochondria were solubilized with 1 % dodecyl-maltoside (DDM) in binding buffer (20  
497 mM HEPES pH 7.4,  $50 \times 10^{-3}$  mol/L NaCl,  $10 \times 10^{-3}$  mol/L MgCl<sub>2</sub>,  $10^{-3}$  mol/L CaCl<sub>2</sub>,  $8 \times 10^{-3}$  mol/L  
498 DTT, 0.1 mg/ml BSA, 10 % glycerol, 0.02 % Tween 20, 1x protease inhibitor cocktail) for 30 min  
499 on ice. 20 µg of biotinylated ssDNA (biotin-5'-  
500 GGACTATTTATTCAATATATTTAAGAATAATTCCAGCTGAGCGCCGG) (60) were added  
501 and incubated on a wheel shaker for 30 min at room temperature. To each reaction, 50 µL of  
502 streptavidin-agarose beads (Sigma-Aldrich) were added and incubated for 30 min at room  
503 temperature. Beads were pelleted at 600g for 1 min and supernatants were collected and  
504 precipitated as described below, while pellets were washed ten times with binding buffer and finally  
505 resuspended in 2x Laemmli buffer. Supernatants were precipitated adding one volume of 20 %  
506 trichloroacetic acid (TCA), washed with cold acetone, air-dried and resuspended in 1X Laemmli  
507 buffer. Pulled-down and supernatant fractions were analyzed by immunoblotting using anti-SSBP1,  
508 anti-VDAC1, anti-HSP60 and anti-ETHE1 antibodies.

509

#### 510 ***Expression and purification of recombinant proteins.***

511 Recombinant baculoviruses encoding POL $\gamma$ B and POL $\gamma$ A were expressed in Sf9 insect cells. These  
512 recombinant proteins lacked the N-terminal mitochondrial targeting sequence and carried a

513 carboxy-terminal 6 × His-tag. The proteins were purified over HIS-Select Nickel Affinity Gel  
514 (Sigma-Aldrich) and HiTrap Heparin HP (GE Healthcare), followed by HiTrap SP HP or HiTrap Q  
515 HP columns (GE Healthcare), depending on the net electrical charge of the protein. SSBP1 lacking  
516 the mitochondrial targeting sequence/MTS (aa 1-16) and containing an N-terminal 6 × His-tag was  
517 expressed in *E. coli* cells and purified over HIS-Select Nickel Affinity Gel (Sigma-Aldrich) and  
518 HiTrap Heparin HP (GE Healthcare), followed by HiTrap SP. Patient point mutations were  
519 introduced using the QuikChange Lightning site-directed mutagenesis kit (Agilent Technologies,  
520 Santa Clara, CA) and verified by sequencing before being expressed and purified as for wt SSBP1.

521

### 522 ***Second strand synthesis assay***

523 A 32P-labelled 50 nt long oligonucleotide (5'-GTG GCA CTT TTC GGG GAA ATG TGC GCG  
524 GAA CCC CTA TTT GTT TAT TTT TC-3') was annealed to single-stranded pBluescript SK II (-).  
525 DNA synthesis assays were performed using 10 fmol template, 200 fmol of POL $\gamma$  holoenzyme and  
526 500 fmol (as tetramer) wt or mutant SSBP1 in 25 × 10<sup>-3</sup> mol/L Tris-HCl (pH 7.8), 10<sup>-3</sup> mol/L TCEP,  
527 10 × 10<sup>-3</sup> mol/L MgCl<sub>2</sub>, 0.1 mg/ml BSA and 10 μM (each) dNTPs. Reactions were incubated at  
528 37 °C for the indicated time and stopped by the addition of 6 μl stop buffer (90 mM EDTA, 6 %  
529 SDS, 30 % glycerol, 0.25 % bromophenol blue and 0.25 % xylene cyanol). Samples were separated  
530 on a 0.8 % agarose gel and visualized by autoradiography.

531

### 532 ***Additional information***

533 The local Ethical Committee in each center approved the study as follows:

534 - University of Bologna: “*Comitato Etico di Area Vasta Emilia Centro della Regione Emilia-*  
535 *Romagna (CE-AVEC) #211/2018/SPER/AUSLBO*” for Families 1, 3 and 4;

536 - Duke University: Duke University Health System Institutional Review Board for Clinical  
537 Investigators (*DUHS IRB, FWA #00009025*), Protocol #32301: Genomic Study of Medical,  
538 Developmental, or Congenital Problems of Unknown Etiology, for Family 2:

539 - University of Innsbruck: Ethical Committee of University of Innsbruck “*Ethikkommission der*  
540 *Medizinischen Universität Innsbruck AN2014-0090 335/4.7*”, for Family 5.  
541 Whole exome sequencing and mtDNA sequencing methods are in Supplemental Material. Genome  
542 data have been deposited at the European Genome-phenome Archive (EGA) which is hosted at the  
543 EBI and the CRG, under accession number EGAS00001003850. Additionally, standard methods for  
544 fluorescence microscopy, oxygen consumption rate, Western blot, assessment of OXPHOS  
545 complexes and respiratory supercomplexes assembly, functional SSBP1 complementation and all  
546 methods related to zebrafish experiments are detailed in the Supplemental Material.

547

#### 548 ***Statistics***

549 GraphPad Prism for Windows (GraphPad Software) was used for statistical analyses. For patients’  
550 tissues and fibroblast’s experiments: comparison of 2 groups was made by unpaired student’s 2-  
551 tailed t-test, whereas for comparisons among multiple groups 1-way or 2-way Anova with Tukey’s  
552 or Dunnett’s multiple comparisons tests have been used. For zebrafish experiments unpaired  
553 student’s 2-tailed t-test and ANOVA with Tukey’s multiple comparisons test have been used. For  
554 all analyses, differences were considered significant at a P value  $\leq 0.05$ .

**Author contributions**

VDD, FU, IDM, PM, MG, AM, LC, FP, FT, BM, ZS, CP, MAG, WCC, IC, CZ, RK, MA, MP, KK and NS carried out the experiments;

CLM, PB, MC, MLV, RL, EB, RC, FE, FDC and VC performed clinical investigation of Families 1, 3 and 4;

VS, JS, SN, ME-D and AI performed clinical investigation of the proband from Family 2;

SB and WS performed clinical investigation of the proband from Family 5;

VDD, FU, IDM, PM, MG, AM, LC, CP, SBW, EED, EHB analyzed and interpreted the data;

VDD, FU, IDM, PM, EED, AI and WCC contributed to study design and reviewed and revised the manuscript;

VC, HP, NK, VT, TP, WC, MS and MF designed and supervised the study, acquired funding and wrote the manuscript.

**Acknowledgments**

This study was supported by the “Ricerca Corrente” funding (AM, LC, FT, FP, MC) and by the Grant GR-2016-02361449 to LC, both from the Italian Ministry of Health; by the German BMBF and Horizon2020 through E-Rare project GENOMIT (01GM1603 to HP and FWF-I 2741-B26) and German Network for Mitochondrial Disorders (mitoNET 01GM1906B to HP); and by the Intramural Research Program of the NIH, National Institute of Environmental Health Sciences (ES065078 to WCC and MAG). The financial support of Mariani Foundation, Milan and of Mitocon – Italy, Grant no. 2018-01 to VT are acknowledged. CP is supported by a fellowship from Associazione Luigi Comini Onlus, Italy. FU and KK were funded by an International Research Support Initiative Program fellowship from the Higher Education Commission of Pakistan. We thank T. Khan for technical assistance with zebrafish experiments. Family 2 was evaluated through

*SSBP1* mutations in optic atrophy with mtDNA depletion

the Duke Genome Sequencing Clinic, supported by the Duke University Health system, and partially funded by UCB Celltech. We thank Dr. Federico Sadun for referring patients from Family 1 and Dott. Rosanna Carroccia for technical help with kidney biopsy of PT1.

**References**

1. Carelli V, et al. Optic neuropathies: the tip of the neurodegeneration iceberg. *Hum Mol Genet.* 2017;26(R2):R139-R150.
2. Yu-Wai-Man P, et al. A neurodegenerative perspective on mitochondrial optic neuropathies. *Acta Neuropathol.* 2016;132(6):789-806.
3. Wallace DC, et al. Mitochondrial DNA mutation associated with Leber's hereditary optic neuropathy. *Science.* 1988;242 (4884):1427-1430.
4. Chan DC. Fusion and fission: interlinked processes critical for mitochondrial health. *Annu Rev Genet.* 2012;46:265-287.
5. Alexander C, et al. OPA1, encoding a dynamin-related GTPase, is mutated in autosomal dominant optic atrophy linked to chromosome 3q28. *Nat Genet.* 2000;26(2):211-215.
6. Delettre C, et al. Nuclear gene OPA1, encoding a mitochondrial dynamin-related protein, is mutated in dominant optic atrophy. *Nat Genet.* 2000;26(2):207-210.
7. Züchner S, et al. Axonal neuropathy with optic atrophy is caused by mutations in mitofusin 2. *Ann Neurol.* 2006;59(2):276-281.
8. Gerber S, et al. Mutations in DNM1L, as in OPA1, result in dominant optic atrophy despite opposite effects on mitochondrial fusion and fission. *Brain.* 2017;140(10):2586-2596.
9. Reynier P, et al. OPA3 gene mutations responsible for autosomal dominant optic atrophy and cataract. *J Med Genet.* 2004;41(9):e110.
10. Abrams AJ, et al. Mutations in SLC25A46, encoding a UGO1-like protein, cause an optic atrophy spectrum disorder. *Nat Genet.* 2015;47(8):926-932.
11. Amati-Bonneau P, et al. OPA1 mutations induce mitochondrial DNA instability and optic atrophy 'plus' phenotypes. *Brain.* 2008;131(Pt2):338-351.

*SSBP1* mutations in optic atrophy with mtDNA depletion

12. Hudson G, et al. Mutation of OPA1 causes dominant optic atrophy with external ophthalmoplegia, ataxia, deafness and multiple mitochondrial DNA deletions: a novel disorder of mtDNA maintenance. *Brain*. 2008;131(Pt2):329-337.
13. Rouzier C, et al. The MFN2 gene is responsible for mitochondrial DNA instability and optic atrophy 'plus' phenotype. *Brain*. 2012;135(Pt1):23-34.
14. Yu-Wai-Man P, et al. Multi-system neurological disease is common in patients with OPA1 mutations. *Brain*. 2010;133(Pt3):771-786.
15. Carelli V, et al. Syndromic parkinsonism and dementia associated with OPA1 missense mutations. *Ann Neurol*. 2015;78(1):21-38.
16. Zeviani M, Servidei S, Gellera C, Bertini E, DiMauro S, DiDonato S. An autosomal dominant disorder with multiple deletions of mitochondrial DNA starting at the D-loop region. *Nature*. 1989;339(6222):309-311.
17. Viscomi C, Zeviani M. MtDNA-maintenance defects: syndromes and genes. *J Inherit Metab Dis*. 2017;40(4):587-599.
18. DiMauro S, Schon EA, Carelli V, Hirano M. The clinical maze of mitochondrial neurology. *Nat Rev Neurol*. 2013;9(8):429-444.
19. Tiranti V, Rocchi M, DiDonato S, Zeviani M. Cloning of human and rat cDNAs encoding the mitochondrial single-stranded DNA-binding protein (SSB). *Gene*. 1993; 126(2):219-225.
20. Tiranti V, et al. Chromosomal localization of mitochondrial transcription factor A (TCF6), single-stranded DNA-binding protein (SSBP), and endonuclease G (ENDOG), three human housekeeping genes involved in mitochondrial biogenesis. *Genomics*. 1995;25(2):559-564.

*SSBP1* mutations in optic atrophy with mtDNA depletion

21. Miralles Fusté J, et al. In vivo occupancy of mitochondrial single-stranded DNA binding protein supports the strand displacement mode of DNA replication. *PLoS Genet.* 2014;10(12):e1004832.
22. Sobreira N, Schiettecatte F, Valle D, Hamosh A. GeneMatcher: a matching tool for connecting investigators with an interest in the same gene. *Hum Mutat.* 2015;36(10):928-930.
23. Baugh EH, et al. Robust classification of protein variation using structural modelling and large-scale data integration. *Nucleic Acids Res.* 2016; 44(6): 2501-2513.
24. Farr CL, Wang Y, Kaguni LS. Functional interactions of mitochondrial DNA polymerase and single-stranded DNA-binding protein. Template-primer DNA binding and initiation and elongation of DNA strand synthesis. *J Biol Chem.* 1999;274(21):14779-14785.
25. Thisse B, and Thisse C. Fast Release Clones: A High Throughput Expression Analysis. ZFIN Direct Data Submission. 2004 (<http://zfin.org>).
26. Carnes MU, et al. Discovery and functional annotation of SIX6 variants in primary open-angle glaucoma. *PLoS Genet.* 2014;10(5):e1004372.
27. Samuel A, Rubinstein AM, Azar TT, Ben-Moshe Livne Z, Kim SH, Inbal A. Six3 regulates optic nerve development via multiple mechanisms. *Sci Rep.* 2016;6:20267.
28. Drummond IA. Zebrafish kidney development. *Methods Cell Biol.* 2004;76:501-30.
29. Hentschel DM, et al. Rapid screening of glomerular slit diaphragm integrity in larval zebrafish. *Am J Physiol Renal Physiol.* 293(5):F1746-50.
30. Anderson BR, et al. In vivo Modeling Implicates APOL1 in Nephropathy: Evidence for Dominant Negative Effects and Epistasis under Anemic Stress. *PLoS Genet.* 6;11(7):e1005349.

*SSBP1* mutations in optic atrophy with mtDNA depletion

31. Spinazzola A, et al. MPV17 encodes an inner mitochondrial membrane protein and is mutated in infantile hepatic mitochondrial DNA depletion. *Nat Genet.* 2006;38(5):570-575.
32. Karadimas CL, et al. Navajo neurohepatopathy is caused by a mutation in the MPV17 gene. *Am J Hum Genet.* 2006;79(3):544-548.
33. Giordano C, et al. Gastrointestinal dysmotility in mitochondrial neurogastrointestinal encephalomyopathy is caused by mitochondrial DNA depletion. *Am J Pathol.* 2008;173(4):1120-1128.
34. Carelli V, et al. Mitochondrial Ophthalmology. In: DiMauro S, Hirano M, Schon EA, eds. *Mitochondrial Medicine.* Abington, Oxon OX14 4RN, UK. Informa Healthcare 2006:105-142.
35. Genead MA, et al. Photoreceptor structure and function in patients with congenital achromatopsia. *Invest Ophthalmol Vis Sci.* 2011;52(10):7298-308.
36. Sundaram V, et al. Retinal Structure and Function in Achromatopsia: Implications for Gene Therapy. *Ophthalmology.* 2014;121(1):234-245.
37. Luo X, et al. Blue cone monochromacy: visual function and efficacy outcome measures for clinical trials. *PLoS One.* 2015;10(4):e0125700.
38. Sergouniotis PI, et al. High-resolution optical coherence tomography imaging in KCNV2 retinopathy. *Br J Ophthalmol.* 2012;96(2):213-7.
39. Moraes CT, et al. mtDNA depletion with variable tissue expression: a novel genetic abnormality in mitochondrial diseases. *Am J Hum Genet.* 1991;48(3):492-501
40. Kullar PJ, et al. Heterozygous *SSBP1* start loss mutation co-segregates with hearing loss and the m.1555A>G mtDNA variant in a large multigenerational family. *Brain.* 2018; 141(1):55-62.

*SSBP1* mutations in optic atrophy with mtDNA depletion

41. Kukat C, Wurm CA, Spåhr H, Falkenberg M, Larsson NG, Jakobs S. Super-resolution microscopy reveals that mammalian mitochondrial nucleoids have a uniform size and frequently contain a single copy of mtDNA. *Proc Natl Acad Sci USA*. 2011;108(33):13534-13539.
42. Kukat C, et al. Cross-strand binding of TFAM to a single mtDNA molecule forms the mitochondrial nucleoid. *Proc Natl Acad Sci U S A*. 2015;112(36):11288-11293.
43. Giordano C, et al. Efficient mitochondrial biogenesis drives incomplete penetrance in Leber's hereditary optic neuropathy. *Brain*. 2014; 137(Pt2):335-353.
44. Spinazzola A, et al. Early-onset liver mtDNA depletion and late-onset proteinuric nephropathy in Mpv17 knockout mice. *Hum Mol Genet*. 2009;18(1):12-26.
45. Zanna C, et al. OPA1 mutations associated with dominant optic atrophy impair oxidative phosphorylation and mitochondrial fusion. *Brain*. 2008;131(Pt2):352-367.
46. Del Dotto V, et al. Deciphering OPA1 mutations pathogenicity by combined analysis of human, mouse and yeast cell models. *Biochim Biophys Acta Mol Basis Dis*. 2018;1864(10):3496-3514
47. Posse V, et al. RNase H1 directs origin-specific initiation of DNA replication in human mitochondria. *PLoS Genet*. 2019;15(1):e1007781.
48. Korhonen JA, Pham XH, Pellegrini M, Falkenberg M. Reconstitution of a minimal mtDNA replisome in vitro. *EMBO J*. 2004;16;23(12):2423-2429.
49. Milenkovic D, et al. TWINKLE is an essential mitochondrial helicase required for synthesis of nascent D-loop strands and complete mtDNA replication. *Hum Mol Genet*. 2013;15;22(10):1983-1993.

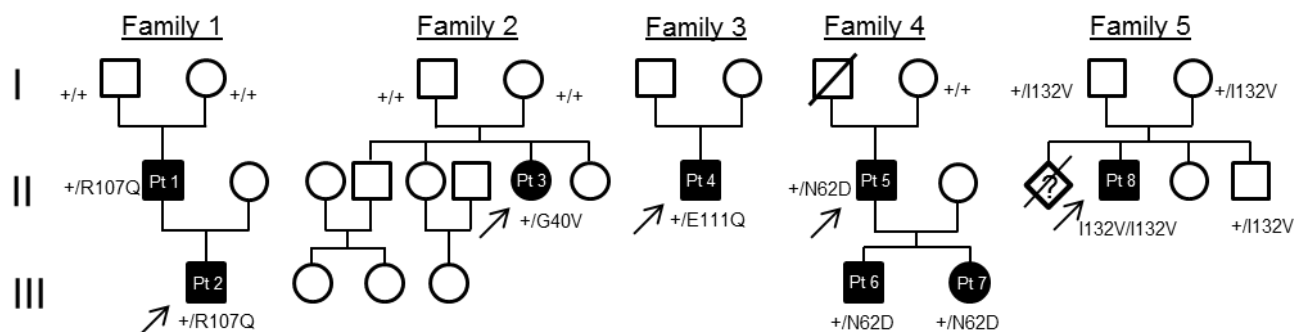
*SSBP1* mutations in optic atrophy with mtDNA depletion

50. Jemt E, et al. Regulation of DNA replication at the end of the mitochondrial D-loop involves the helicase TWINKLE and a conserved sequence element. *Nucleic Acids Res.* 2015;43(19):9262-9275.
51. Antes A, et al. Differential regulation of full-length genome and a single-stranded 7S DNA along the cell cycle in human mitochondria. *Nucleic Acids Res.* 2010;38(19):6466-6476.
52. Reyes A, et al. RNASEH1 Mutations Impair mtDNA Replication and Cause Adult-Onset Mitochondrial Encephalomyopathy. *Am J Hum Genet.* 2015;97(1):186-193.
53. Kornblum C, et al. Loss-of-function mutations in MGME1 impair mtDNA replication and cause multisystemic mitochondrial disease. *Nat Genet.* 2013;45(2):214-219.
54. Mussini C, et al. Effect of treatment interruption monitored by CD4 cell count on mitochondrial DNA content in HIV-infected patients: a prospective study. *AIDS.* 2005;19(15):1627-1633.
55. Krishnan KJ, Bender A, Taylor RW, Turnbull DM. A multiplex real-time PCR method to detect and quantify mitochondrial DNA deletions in individual cells. *Anal Biochem.* 2007;370(1):127-129.
56. Hjerpe R, et al. Oligomerization conditions Mdm2-mediated efficient p53 polyubiquitylation but not its proteasomal degradation. *Int J Biochem Cell Biol.* 2010;42(5):725-735.
57. Fernández-Vizarra E, López-Pérez MJ, Enriquez JA. Isolation of biogenetically competent mitochondria from mammalian tissues and cultured cells. *Methods.* 2002;26(4):292-297.
58. Lyonais S, et al. The human mitochondrial transcription factor A is a versatile G-quadruplex binding protein. *Sci Rep.* 2017;7:43992.

*SSBP1* mutations in optic atrophy with mtDNA depletion

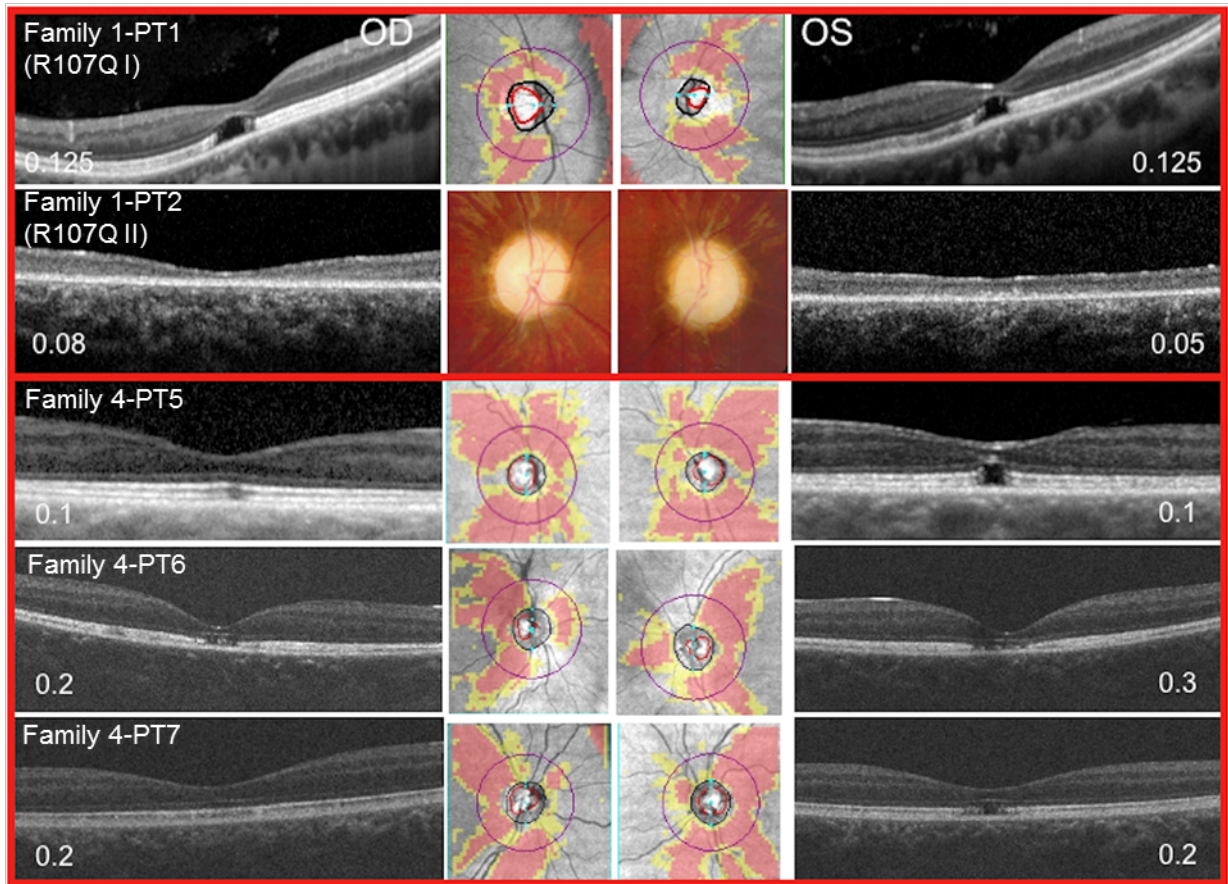
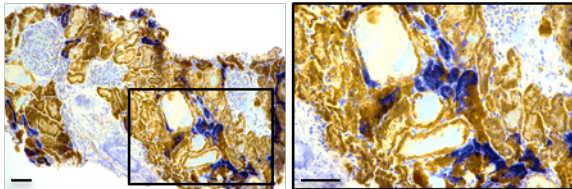
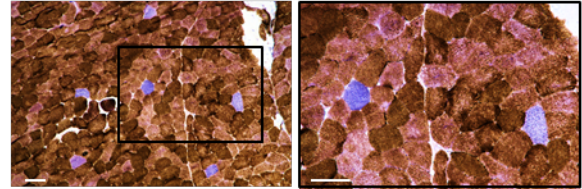
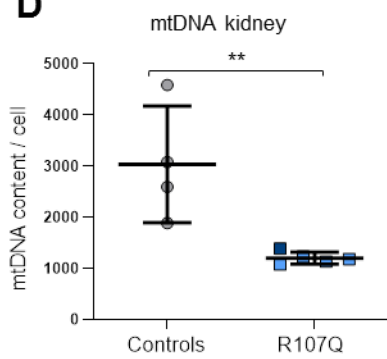
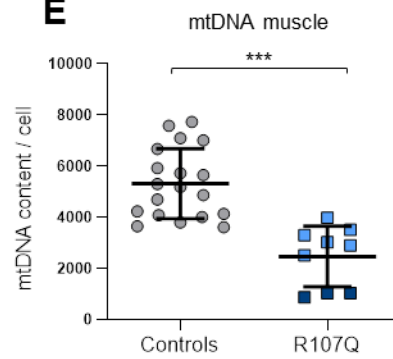
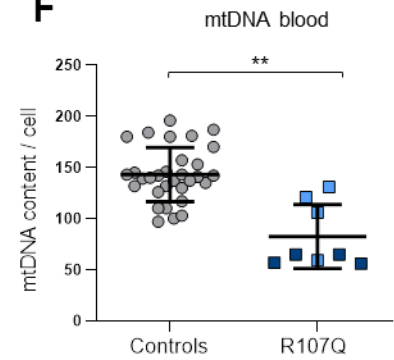
59. Lu B, et al. Phosphorylation of human TFAM in mitochondria impairs DNA binding and promotes degradation by the AAA+ Lon protease. *Mol Cell*. 2013;49(1):121-132.
60. Ciesielski GL, Rosado-Ruiz FA, Kaguni LS. Purification and Comparative Assay of Human Mitochondrial Single-Stranded DNA-Binding Protein. *Methods Mol Biol*. 2016;1351:211-222.
61. Jay JJ, Brouwer C. Lollipops in the Clinic: Information Dense Mutation Plots for Precision Medicine. *PLoS One*. 2016;11(8):e0160519.
62. Traynelis J, Silk M, Wang Q, Berkovic SF, Liu L, Ascher DB, Balding DJ, Petrovski S. Optimizing genomic medicine in epilepsy through a gene-customized approach to missense variant interpretation. *Genome Res*. 2017;27(10):1715-1729.

### Figures and Figure Legends



**Figure 1. Pedigrees of the 5 families carrying SSBP1 mutations.** Affected individuals (black-filled circles/squares) present with variable combination of optic atrophy with clinical phenotypes including retinal dystrophy, kidney insufficiency, mitochondrial myopathy among others. All mutations segregate consistently with the disease phenotype.

## SSBP1 mutations in optic atrophy with mtDNA depletion

**A****B****C****D****E****F**

**Figure 2. OCT, muscle and kidney histopathology and tissue's mtDNA quantification of patients carrying *SSBP1* mutations**

(A) Macular and optic nerve OCT and visual acuity of patients from Families 1 and 4.

Family1-PT1 patient shows a complete foveal cavitation characterized by the absence of inner segment/outer segment and outer segment/ RPE junctions. Family1-PT2 patient shows diffuse atrophy of the photoreceptors' layers.

Family 4-PT5 patient shows incomplete (OD) and complete (OS) foveal cavitation. Family 4-PT6 patient shows incomplete foveal cavitation characterized by partial disruption of inner/outer segment and outer segment/RPE junctions. Family 4-PT7 patient shows mild rarefaction of the hyper-reflectivity of the inner segment/outer segment junction (OD) and incomplete form of foveal cavitation (OS).

Optic disc atrophy is documented by the diffuse retinal nerve fiber layer thinning in the OCT deviation map of the optic nerve (middle) or in the color optic nerve picture.

(B) Kidney and (C) muscle histochemistry of proband PT1 of Family 1 (R107Q I). COX/SDH staining reveals COX negative cells in the tubular component of kidney parenchyma and in sporadic muscle fibers. Boxes on merged images correspond to magnified insets. Scale bar, 100 $\mu$ m.

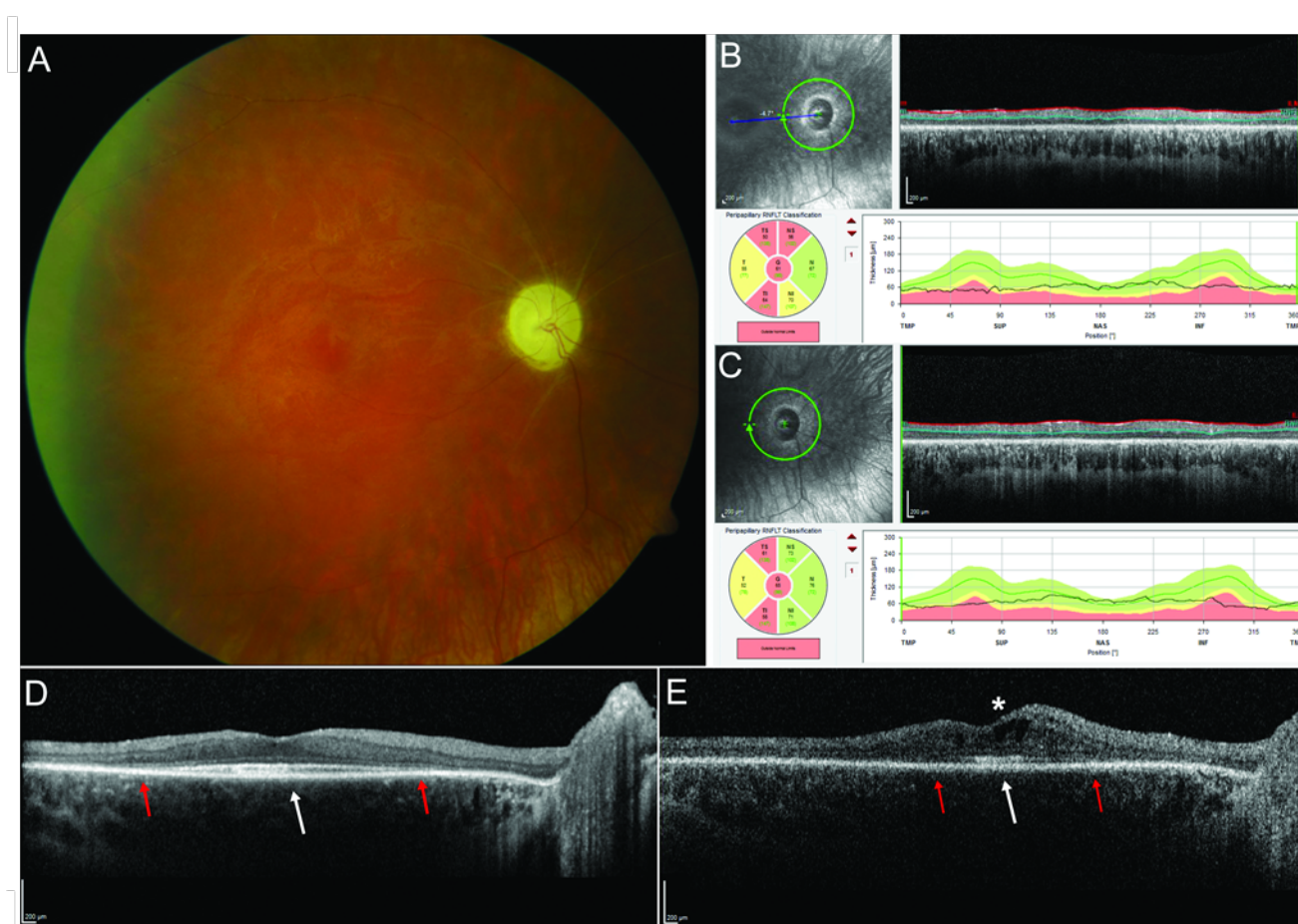
(D-F) mtDNA copy number from different tissues of healthy individuals (controls) and the PT1 and PT2 patients from Family 1: proband (R107Q I, light blue) and his son (R107Q II, dark blue).

(D) Data are shown as mean  $\pm$  SD of 4 controls and patients (1 experiment for R107Q I and 3 experiments for R107Q II).

(E) Data are shown as mean  $\pm$  SD of 19 controls and patients (2 biopsies of R107Q I analyzed in 6 experiments, and 3 experiments for R107Q II).

(F) Data are shown as mean  $\pm$  SD of 31 controls and R107Q patients (2 blood samples for patients, analyzed in 4 experiments).

A reduction of mtDNA content was observed in patient's tissues. \*\* and \*\*\* denotes  $p < 0.01$  and  $p < 0.001$ , respectively, using student's 2-tailed t test.

*SSBP1* mutations in optic atrophy with mtDNA depletion

**Figure 3. Ophthalmologic phenotype associated with the p.G40V *SSBP1* mutation.** In all panels, the right eye (OD) is illustrated as representative of both eyes. Disease expression in this proband ascertained at Duke (PT3) was symmetric.

(A) Ophthalmoscopy showed diffuse optic nerve pallor, blunted foveal reflexes but enhanced vitreoretinal interface reflexes, and marked vasculature attenuation with ghost vessel-like appearance.

(B) RNFL OCT scan obtained at the age of 17 yr, 10 months: the average RNFL thickness was only ~60-65  $\mu\text{m}$  in each eye.

(C) At age 23 years old, there was no significant change in the extent of the RNFL loss.

(D) The macular OCT obtained at the age of 17 yr, 10 months shows mild thinning of all retinal layers and marked loss of the ellipsoid zone (red arrows) with foveal sparing and presence of subfoveal hyperreflectivity at the EZ/RPE interface (white arrow).

*SSBP1* mutations in optic atrophy with mtDNA depletion

(E) Follow-up macular OCT at age 23 years old showed significant increase in the thinning of all retinal layers, further contraction of the EZ residue (red arrows) but persistent subfoveal hyperreflectivity (white arrow). Hyporefective cystic spaces consistent with macular edema had developed at this age as well (white asterisk).

*SSBP1* mutations in optic atrophy with mtDNA depletion

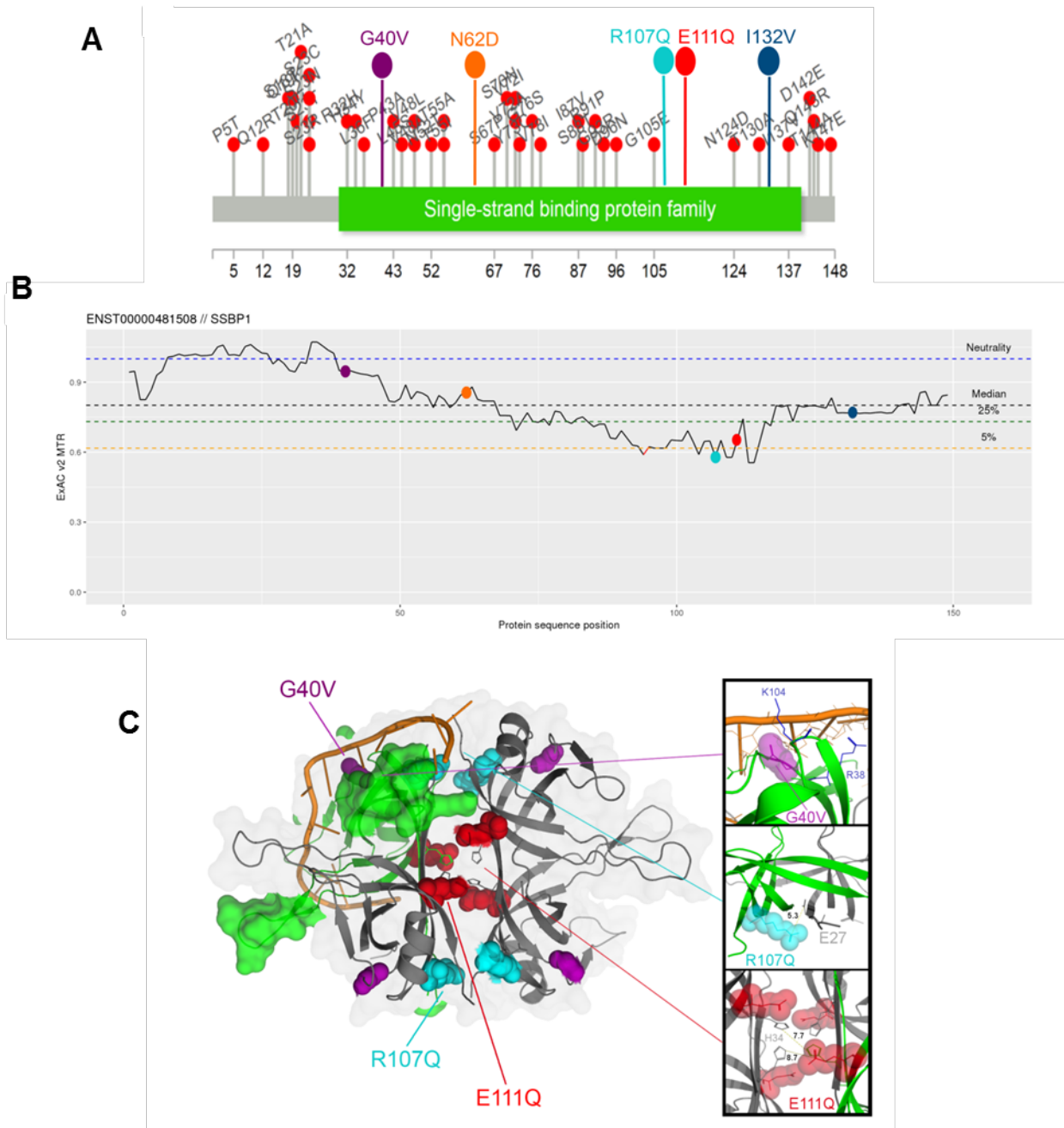


**Figure 4. Distribution of *SSBP1* mutations and protein in silico model.**

(A) “Lollipop”(61) diagram of ultra-rare population and patients’ variants along the protein: variants with  $\leq 2$  gnomAD alleles are represented by grey sticks with red circles on top, while patients’ variants sticks and circles are uniformly colored. The green box is the SSB domain.

(B) Missense Tolerance Ratio diagram for SSBP1 and location of patients’ variants: Missense Tolerance Ratio (MTR) viewer v0.3(62) was used with window size 31 on ENST00000481508 transcript. MTR is plotted against SSBP1 sequence, and locations of variants are represented with

*SSBP1* mutations in optic atrophy with mtDNA depletion

dots using the same color code as in panel B. Dotted lines represent neutrality (blue) or different percentiles - black (median), green (25<sup>th</sup>), yellow (5<sup>th</sup>) - of most missense depleted gene regions.

(C) Structural Model of the SSBP1 homotetramer (from PDB code 3ULL) with aligned ssDNA (from structural alignment to 3ULP): the three positions carrying the most deleterious predictions are highlighted on wt homotetramer with same color code as panels B/C. *Upper inset*) Gly40 occurs close to the approximate ssDNA binding site, not directly contacting DNA but forming a highly constrained loop coordinating DNA-contacting residues Arg38 and Lys104. *Middle Inset*) Arg107 occurs on the outer surface of the homotetramer at both homodimeric and homotetrameric interfaces. It is spatially close to Glu27 (5.3°A away) and likely forms a stabilizing salt-bridge across dimer interface. *Lower inset*) Glu111 occurs directly in the tetrameric interface and potentially forms a stabilizing salt-bridge with His34 although the available model does not clearly indicate the monomer this interaction occurs with (both His34 residues on opposing dimer are spatially close to Glu111, 7.7°A and 8.7°A, respectively).

## SSBP1 mutations in optic atrophy with mtDNA depletion

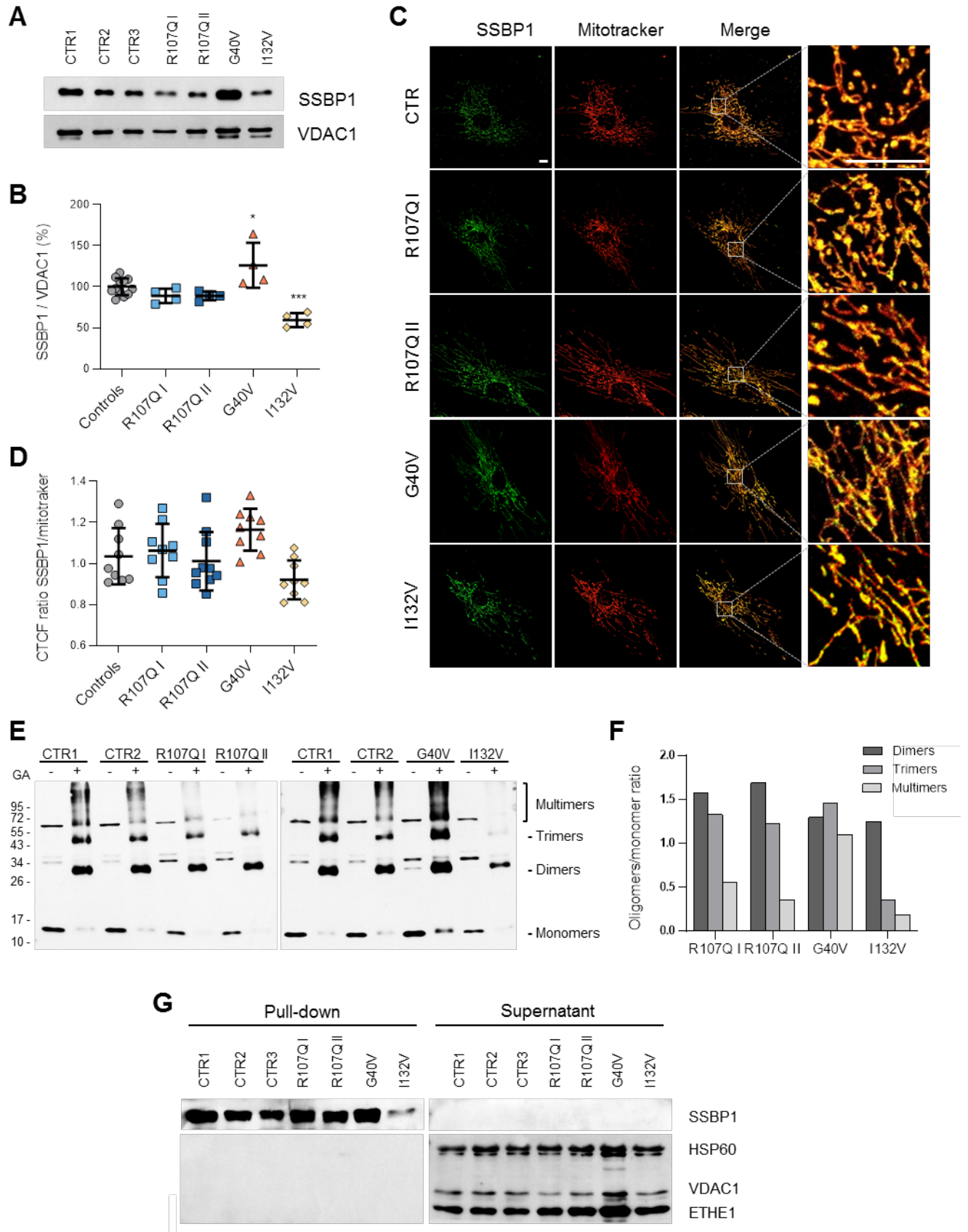


**Figure 5. Effect of *SSBP1* mutations on protein stability, oligomerization and ssDNA binding in fibroblasts.**

*SSBP1* mutations in optic atrophy with mtDNA depletion

(A) Western blot analysis of SSBP1 expression levels on isolated mitochondria; VDAC1 was used as a loading control. A representative blot out of four independent experiments is shown.

(B) Densitometric analysis of four independent Western blot experiments shows an increase and a reduction of SSBP1 level in G40V and I132V cells, respectively. All values (means  $\pm$  SD) are normalized to control cells. n = 12 (controls) and 4 (mutants).

(C) Representative confocal images of fibroblasts labeled with anti-SSBP1 antibody (green) and MitoTracker red (red). Boxes on merged images correspond to magnified insets at right of each panel. Scale bar, 10  $\mu$ m.

(D) Quantification of SSBP1-MitoTracker co-localization, expressed as Corrected Total Cell Fluorescence (CTCF) ratio on nine images per group. Data are means  $\pm$  SD.

(E) SSBP1 oligomerization analysis performed on the same samples used in (A). GA: 0,1% glutaraldehyde. The presence of monomeric (molecular weight around 15kDa), dimeric (molecular weight around 30kDa), trimeric (molecular weight around 45kDa) and multimeric (molecular weights >60kDa) forms are indicated. The protein amount utilized for the different samples was previously determined for Western blot analysis in Figure 3A.

(F) Densitometric analysis of (E) shows that p.R107Q and p.I132V mutations, but not p.G40V, interfere with SSBP1 multimerisation. All values represent the ratio between each oligomer amount in presence of GA and monomers without GA.

(G) SSBP1-ssDNA binding assay performed on isolated mitochondria shows that SSBP1 mutants were able to bind ssDNA. Streptavidin-agarose beads were used to precipitate biotinylated ssDNA together with associated proteins. Supernatants and pull-down fractions were run on a SDS-PAGE and immune-blotted with anti-SSBP1, anti-VDAC1, anti-HSP60 and anti-ETHE1 antibodies. A representative blot out of three is shown.

\*, \*\* and \*\*\* denotes  $p < 0.05$ ,  $p < 0.01$  and  $p < 0.001$ , respectively. Statistical significance was determined using 1-way ANOVA with Tukey's correction.

## SSBP1 mutations in optic atrophy with mtDNA depletion

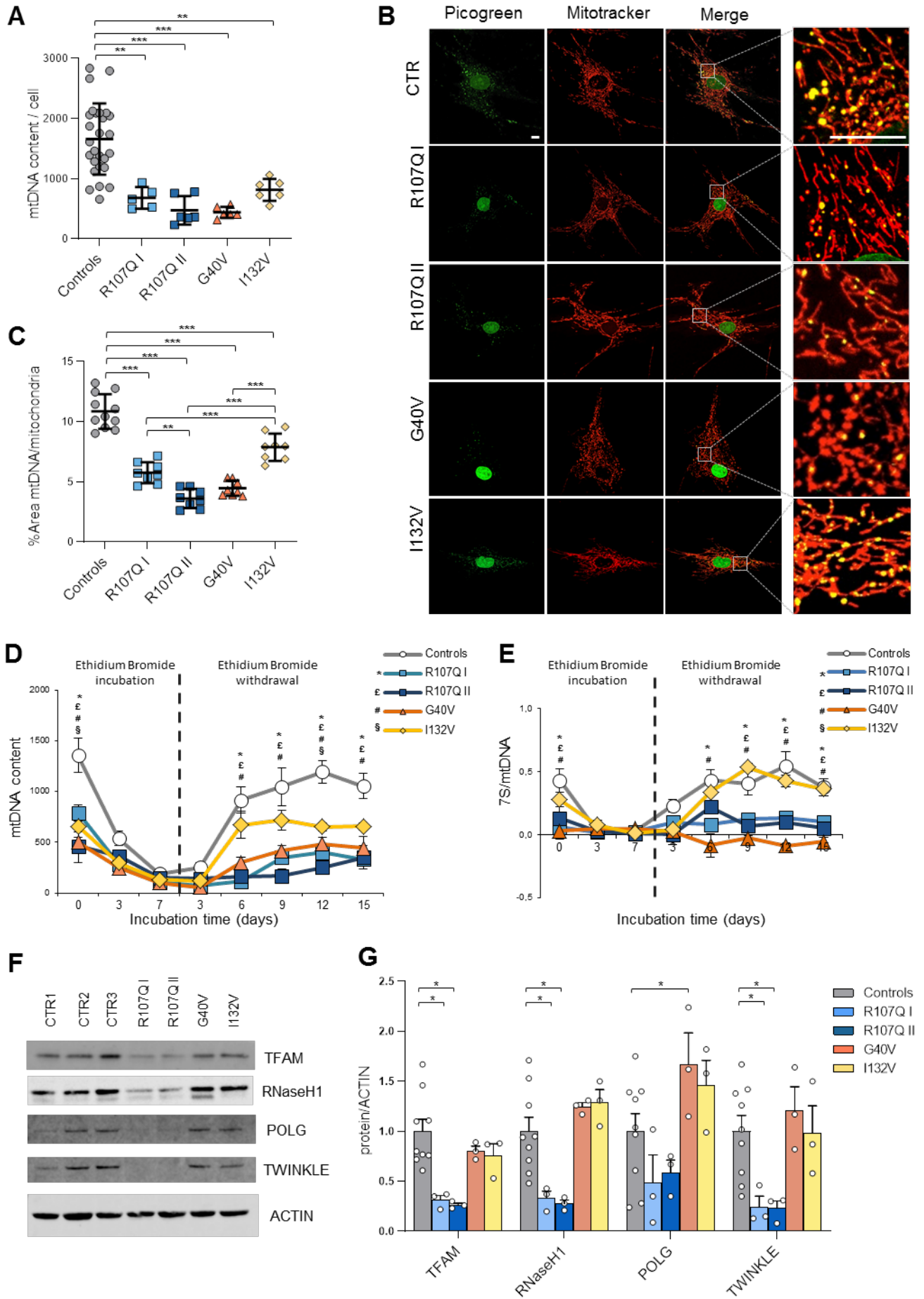


**Figure 6. Effect of *SSBP1* mutation on mtDNA amount, nucleoids and on the dynamics of genome repopulation in fibroblasts.**

(A) mtDNA copy number quantification reveals a depletion in all mutant cells. Data are means  $\pm$  SD of controls (n=21), mutants (n=6) except for R107Q I (n=5).

(B) Representative live confocal images of fibroblasts labeled with Picogreen (green) and MitoTracker red (red). Boxes on merged images correspond to magnified insets at right of each panel. Scale bar, 10  $\mu$ m.

(C) Quantification of nucleoids, expressed as the ratio between the percentage of the area occupied by nucleoids (Picogreen, nuclei excluded) and the area occupied by mitochondria (MitoTracker), shows a significant reduction of nucleoids number in all mutant cell lines. Data are means  $\pm$  SD of controls (n=11) and mutants (n=9).

(D) Mitochondrial DNA repopulation after depletion by ethidium bromide in fibroblasts. mtDNA content is shown as mean  $\pm$  SEM of controls (n=7) and mutant cells (n=3). A severe effect is observed for p.R107Q and p.G40V cells. \*,£,# and § denote values significantly different from the controls (p<0.05) of R107Q I, R107Q II, G40V and I132V cells, respectively.

(E) Quantification of 7S in the same samples analyzed in (D) reveals a marked reduction in p.R107Q and G40V cells. Data are means  $\pm$  SEM. \*,£,# and § denote values significantly different from the controls (p<0.05) of R107Q I, R107Q II, G40V and I132V cells, respectively.

(F) Western blot of TFAM, RNaseH1, POL $\gamma$  and TWINKLE expression levels; ACTIN was used as a loading control. A representative blot out of three is shown.

(G) Densitometric analysis of (F) shows a reduction of some of the replisoma proteins in p.R107Q cells. All values (means  $\pm$  SEM) are normalized to the control cells.

\*, \*\* and \*\*\* denotes p<0.05, p<0.01 and p<0.001, respectively. Statistical significance was determined using 1-way ANOVA (A, D, E) or 2-way ANOVA (G) with Dunnett's correction, or 1-way ANOVA with Tukey's correction (C).

*SSBP1* mutations in optic atrophy with mtDNA depletion

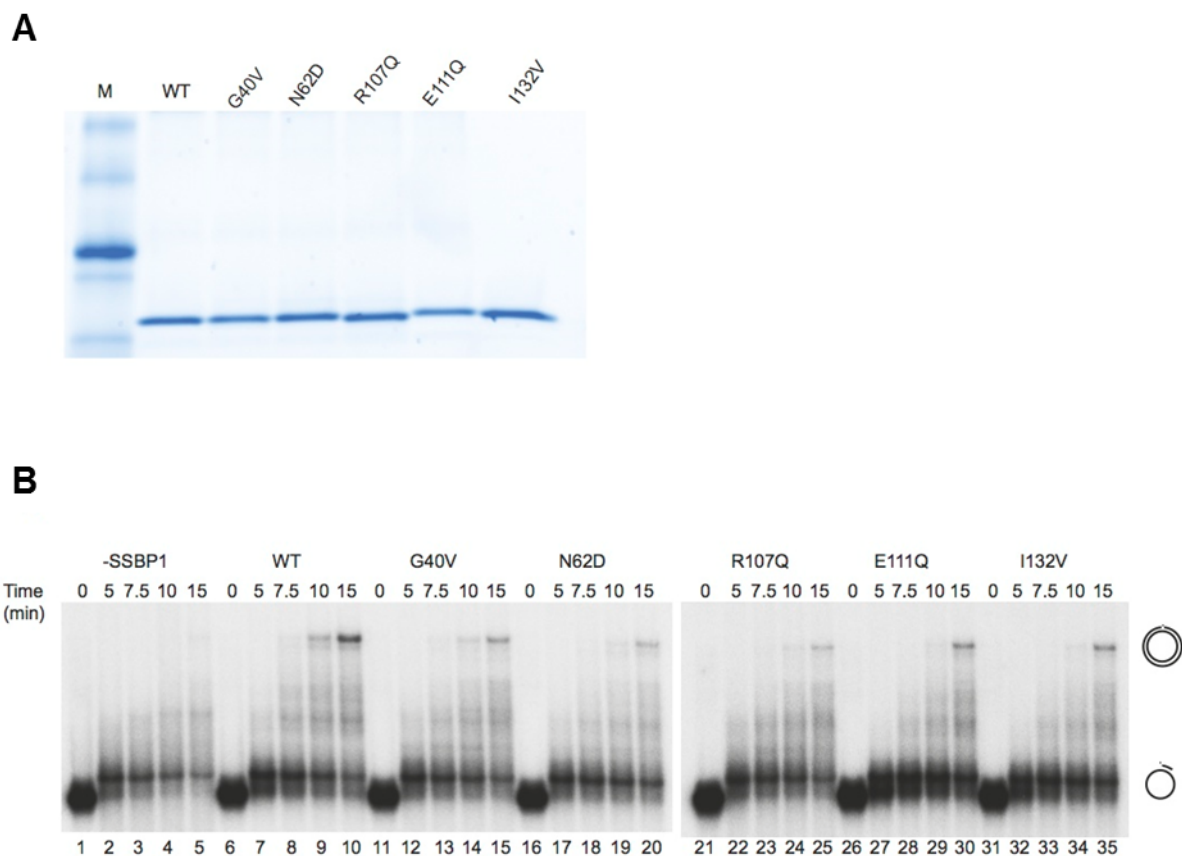


**Figure 7. Effect of mutated SSBP1 protein on DNA replication *in vitro*.**

(A) Ten pmoles of each purified SSBP1 version were separated on SDS-PAGE. M=marker.

(B) DNA polymerase assay performed on a primed single stranded circular DNA shows that all tested mutants displayed a lower stimulatory effect on DNA synthesis than the wt SSBP1.

## SSBP1 mutations in optic atrophy with mtDNA depletion

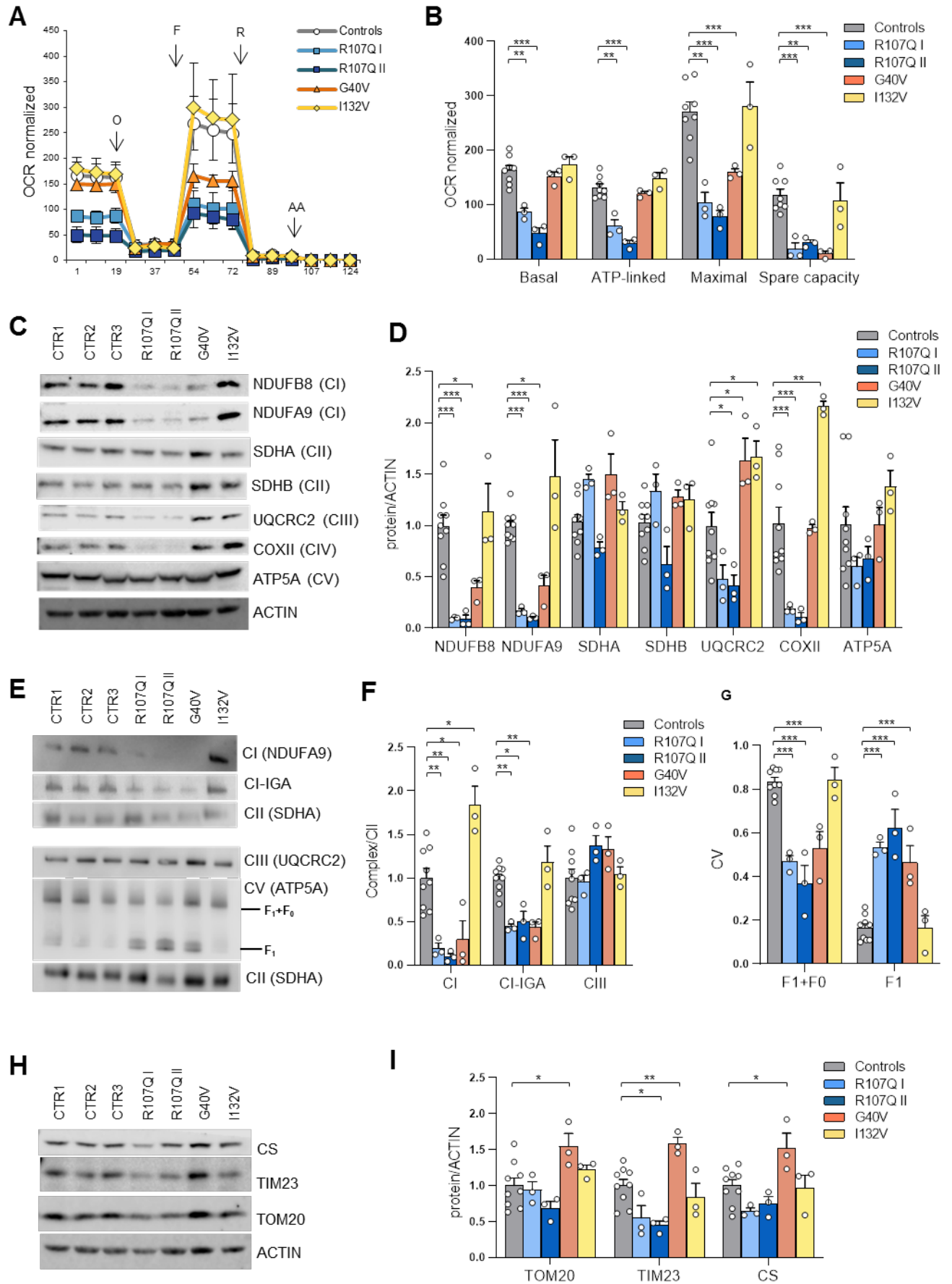


**Figure 8. Energetic profile of *SSBP1* mutated fibroblasts.**

(A) OCR of fibroblasts, expressed as pmoles O<sub>2</sub>/min normalized for protein content, under basal conditions and after injection of oligomycin (O), carbonyl cyanide 4-(trifluoromethoxy) phenylhydrazone (FCCP; F), rotenone (R) and antimycin A (AA). Data are means  $\pm$  SEM of control (n=7) and mutant cells (n=3).

(B) Basal, ATP-linked, maximal respiration and spare respiratory capacity were calculated from OCR traces and are reported in the graph as means  $\pm$  SEM. OCR experiments show a severe reduction of respiratory capacity in p.R107Q and a partial defect in p.G40V mutants.

(C) Western blot of OXPHOS subunits expression levels; ACTIN was used as a loading control. A representative experiment out of three is shown.

(D) Densitometric analysis of (C) shows a variably reduction of OXPHOS subunits in p.R107Q and p.G40V cells. Data, normalized to the control cells, are means  $\pm$  SEM of three independent experiments.

(E) Analysis of complexes assembly was carried out in digitonin-treated mitoplasts resolved by CN and BN-PAGE, as described in Materials and Methods. SDHA (CII) was used as a loading control. A representative experiment out of three is shown.

(F) Densitometric analysis of CI and CIII complexes. Data are means  $\pm$  SEM of three independent experiments.

(G) Densitometric analysis of CV complex, showing an increase of F<sub>1</sub> subunit not assembled in R107Q and G40V fibroblasts.

(H) Western blot of CS, TIM23 and TOM20; ACTIN was used as a loading control. A representative experiment out of three is shown.

(I) Densitometric analysis of the mitochondrial mass proteins. Data, normalized to the control cells, are means  $\pm$  SEM of three independent experiments.

\*, \*\* and \*\*\* denote values significantly different from controls using 1-way (G) or 2-way ANOVA (B, D, F, I) with Dunnett's test ( $p < 0.05$ ,  $p < 0.01$  and  $p < 0.001$ , respectively).

*SSBP1* mutations in optic atrophy with mtDNA depletion

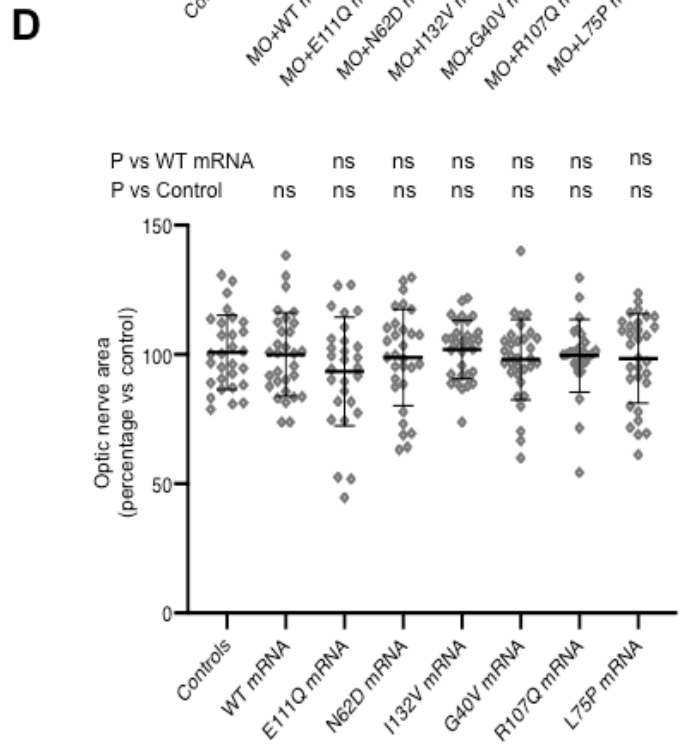
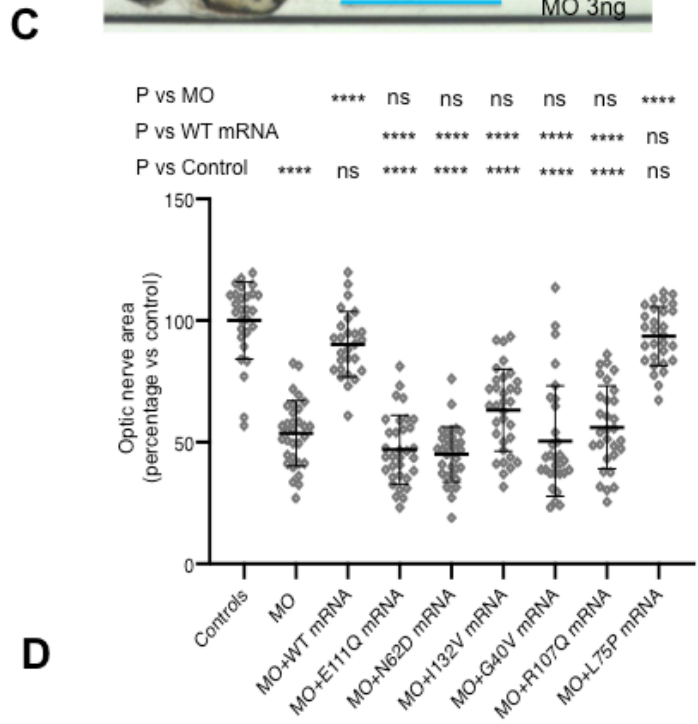
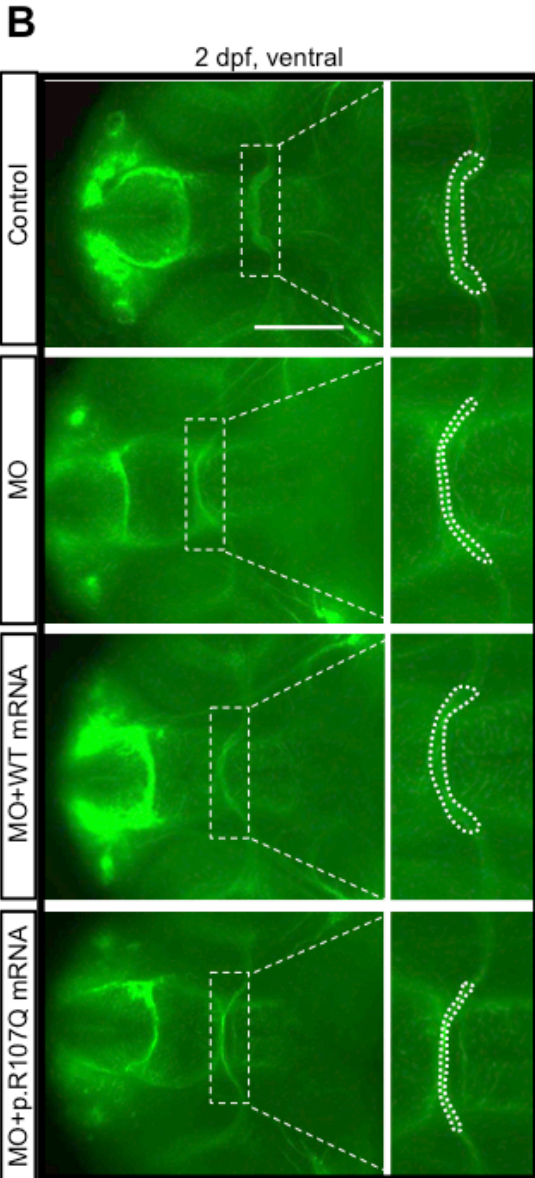
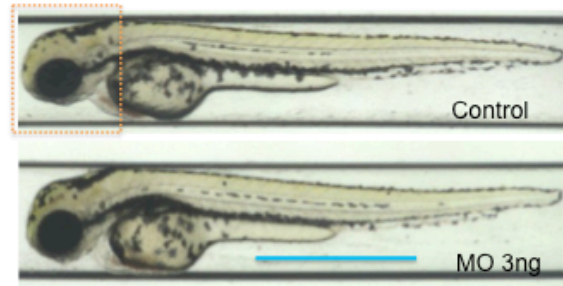
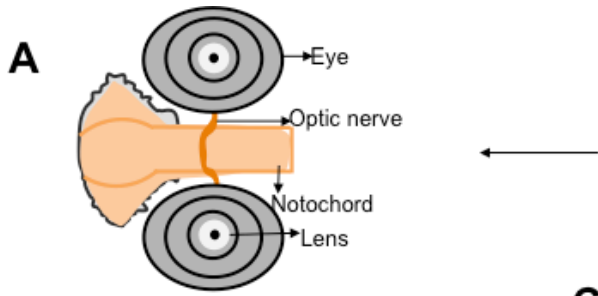


**Figure 9. Optic nerve phenotypes and *in vivo* complementation studies in zebrafish *ssbp1* models**

(A) Left, schematic representation of the ventral view of a 2-day post fertilization (dpf) embryo showing the optic chiasm framed by the notochord as demarcated by acetylated tubulin staining. Right, representative lateral view of 2 dpf larvae (control and *ssbp1* morphant) with the anterior region outlined by a dashed box. Scale bar, 800  $\mu\text{m}$ .

(B) Representative ventral images of whole mount 2 dpf embryos stained with anti-acetylated tubulin antibody to mark the optic nerve. Dashed box corresponds to magnified inset at right of each panel. Region measured is indicated in inset with a white dashed line outlining the area of the optic chiasm. Scale bar, 50  $\mu\text{m}$ .

(C) Quantification of the optic chiasm area in embryo batches (as indicated in panel A). WT mRNA ameliorated MO phenotype significantly, while mRNA harboring patient mutations fails to rescue MO phenotypes. L75P is a negative control variant (rs78598246, 5 homozygotes in gnomAD; accessed Jan 2019). Three biological replicates.

(D) Quantification of the optic chiasm area in embryo batches after overexpression of mRNA; optic nerve phenotypes are not affected.

In panels C and D, \*\*\*\* $p < 0.0001$  denotes significant differences detected by ANOVA with Tukey's multiple comparisons test; ns; not significant;  $n = 26-35$  embryos/batch, three biological replicates gave similar results. Error bars represent SEM.